UC Santa Cruz
UC Santa Cruz Electronic Theses and Dissertations

Title

Centromere-independent Mechanisms of Chromosome Congression and Separation

Permalink

https://escholarship.org/uc/item/1hw5q25h

Author

Vicars, Hannah

Publication Date

2023

Peer reviewed|Thesis/dissertation

UNIVERSITY OF CALIFORNIA
SANTA CRUZ

**CENTROMERE-INDEPENDENT MECHANISMS
OF CHROMOSOME CONGRESSION AND SEPARATION**

A dissertation submitted in partial satisfaction
of the requirements for the degree of

DOCTOR OF PHILOSOPHY

in

MOLECULAR, CELL AND DEVELOPMENTAL BIOLOGY

by

Hannah M. Vicars

December 2023

The Dissertation of Hannah Vicars is approved by:

_____
Professor William Sullivan, Chair

_____
Professor John Tamkun

_____
Professor Susan Strome

_____
Professor William Saxton

_____
Peter Biehl
Vice Provost and Dean of Graduate Studies

Table of Contents

List of Figures

List of Tables

ABSTRACT

CENTROMERE-INDEPENDENT MECHANISMS OF CHROMOSOME CONGRESSION AND SEPARATION

Hannah M. Vicars

The kinetochore has been viewed as playing a critical role in many aspects of chromosome dynamics as the cell progresses through mitosis. This includes chromosome congression and alignment on the metaphase plate and sister chromosome separation and segregation to the spindle poles. Defects in kinetochore function result in mitotic errors and aneuploidy. Thus, the finding that chromosome fragments lacking a kinetochore (acentrics) are capable of normal congression, sister separation and segregation is fascinating. My thesis takes advantage of a *Drosophila* system in which acentrics can be efficiently generated and their behavior analyzed through live fluorescence analysis.

In Chapter 1, we review how cells transmit chromosomes through mitosis without canonical kinetochore-microtubule interactions. Decades of research and a collection of studies reveal that microtubule-based mechanisms and DNA-based "tethers" connecting the acentric to the main chromosome mass are responsible for proper segregation of acentrics.

In Chapter 2, we discuss the mechanisms by which acentric sister chromatids remain paired and eventually separate from one another during anaphase. Taking advantage of *Drosophila* transgenic for the I-CreI endonuclease, we efficiently generate broken chromosome fragments lacking centromeres, thereby lacking kinetochores. By using a genetic screen and live analysis, we identify proteins responsible for the separation of acentric chromosomes. We conclude DNA catenations are responsible for keeping acentric sisters paired and Topoisomerase II activity and microtubule plus-end

pushing forces are needed to resolve these catenations and separate the acentrics.

In Chapter 3, we highlight the remarkable ability of acentrics to congress to the metaphase plate despite the absence of kinetochore-microtubule interactions. Through mutational and live cell analysis, we define the forces acting on chromosome arms and the role of the kinetochore in chromosome congression. Utilizing *Drosophila* with fluorescently tagged acentric X chromosomes, we find acentric chromosome congression relies on interpolar microtubules as well as polar ejection forces. Our studies also show the induction of the DNA damage response leads to a global reorganization of congressed chromosomes at metaphase.

Overall, this dissertation reveals a previously unsuspected kinetochore-independent backup mechanism by which chromosome fragments are able to progress normally through the initial stages of mitosis. Just as the discovery of cell cycle checkpoints led to new insights into the origins of cancer and novel therapies, it is likely that these and future insights into the transmission of chromosome fragments will have a similar impact on basic and applied cancer research.

ACKNOWLEDGEMENTS

I would first like to thank my advisor, Bill, for his unwavering support while I worked in his lab as an undergrad and throughout grad school. Bill has always encouraged me to push myself out of my comfort zone and has seen greatness in me when I did not see it in myself. I am appreciative of his patience and sensitivity surrounding the struggles faced by women in science.

I would also like to thank Travis and Brandt for mentoring me in the lab when I was an undergrad and grad student. They opened my eyes to the fascinating world of cell biology. Thank you to all other current and past lab members who have made working in lab so enjoyable and full of laughter.

Thank you, John for advising me through my teaching experiences and for exemplifying a compassionate instructor and colleague. I will always cherish our lengthy discussions, especially those about pencils and other stationery products.

Thank you to my thesis committee members, Bill and Susan, for providing invaluable feedback on my work. Our thesis committee meetings were always highly productive and fun.

I am incredibly blessed to have such loving and supportive parents. They fostered my science identity from a young age from playing with at-home science experiments to helping me with school science projects. My appreciation of their

support cannot be put into words. I am fortunate to be able to call my parents my best friends. I would certainly not be where I am today without them. I would also like to thank Brother for his support and for helping shape me into the person I am today. Additionally, I would like to acknowledge the support my cousin Lynda and her husband Bruce have given me throughout undergrad and grad school. Hearing Lynda's stories of her journey as a woman in science inspired me when I struggled to see myself as a scientist.

Thank my friends for supporting me through undergrad and grad school, especially Dolly and Parissa. There is no one else with whom I would have rather braved undergrad and grad school. I hope for many more years of friendship.

Finally, I received tremendous support from my dogs, Teddy Bear, Sophie, Lila, and Maya. I am grateful for your unconditional affection and for having the opportunity to share a home with you and go on adventures together. I have also been fortunate to share a home with Lucy (Goose). I appreciate all the affection you have given your Auntie. I would also like to thank my parents' dogs Raina and Mailee for their playfulness and companionship.

Chapter 1: Kinetochore-independent mechanisms of chromosome transmission

Abstract

The kinetochore is a vital macromolecular structure that drives chromosome behavior throughout mitosis. In the absence of kinetochores during mitosis, chromosomes are predicted to fail to align at the metaphase plate, fail to separate and segregate in anaphase, and produce aneuploid daughter cells leading to cell death or cancer. However, studies in various organisms have shown that chromosomes lacking kinetochores, referred to as acentrics, have the exceptional ability to be transmitted through mitosis, producing euploid daughter cells. While canonical chromosome dynamics require end-on attachments of microtubules to kinetochores, cells have developed fascinating strategies to transmit acentric chromosomes through cell division. This review discusses the current literature surrounding the mechanisms by which the cell transmits acentric chromosomes through mitosis, including DNA-based connections and non-canonical microtubule interactions.

Introduction

The kinetochore is a key molecular machine of the eukaryotic chromosome. Studies have shown the kinetochore drives chromosome dynamics throughout all stages of the cell cycle [62]. Thus, it is surprising that chromosome fragments lacking kinetochores, termed acentrics, are capable of normal transmission throughout the cell cycle. In this chapter, we summarize the role of kinetochore and microtubule interactions that guide chromosomes through mitosis. We then describe recent findings on the incredible behavior of acentric

chromosomes and how these findings inform us on the forces and mechanisms driving mitotic chromosome dynamics.

Kinetochore-microtubule interactions drive chromosome transmission through mitosis

The goal of mitosis is to produce genetically identical daughter cells. To achieve this goal, a cell must effectively replicate, organize, separate, and segregate its genome. Leading up to the metaphase-to-anaphase transition, sister chromatid cohesion is maintained by DNA catenations until resolution by Topoisomerase II (Topo II) and cohesin, a tripartite ring-like protein complex comprised of two structural maintenance of chromosome proteins (SMC1, SMC3) and a kleisin subunit (Rad21/Scc1) [30, 58, 79].

While remaining paired together, sister chromatids travel to the metaphase plate in early mitosis. Sister chromatids that are oriented parallel to the mitotic spindle are initially carried to a spindle pole by dynein [53]. Once at the spindle pole, sister kinetochores interact with plus-end-directed CENP-E and sister chromatid arms interact with chromokinesins to align at the spindle equator. This process is known as peripheral chromosome congression [53]. If sister chromatids are oriented perpendicular to the spindle during prometaphase, they will travel to the metaphase plate via end-on attachments of microtubules to their kinetochores. During this direct congression, chromokinesins will also help guide chromosome arms to metaphase [53]. Interestingly, it has been found that chromosome congression is dependent on kinetochore size [17]. Chromosomes with larger kinetochores are less dependent on CENP-E activity and undergo congression after biorientation to the spindle [17]. The balance of kinetochore pulling forces and polar ejection forces on chromosome arms help drive

2

chromosome movement in congression to the metaphase plate and during segregation in anaphase.

At the spindle assembly checkpoint, the cell ensures that proper microtubule-kinetochore biorientation has been achieved [97]. Topo II decatenates intertwined DNA allowing sisters to separate and segregate to opposing cell poles [79]. Additionally, cohesin complexes are first removed from chromosome arms through proteolytic cleavage of the kleisin subunit by separase [67, 80, 104, 105]. Due to the Sgo/PP2A-dependent protection mechanism, cohesin remains at the centromeric regions [31]. Entry into anaphase is controlled by CDK1 activation of the anaphase-promoting complex/cyclosome (APC/C). This results in cyclin degradation, cohesin removal, and resolution of DNA catenations. Microtubule-kinetochore attachments can then drive sister chromatid separation and poleward segregation [3, 68].

The importance of the kinetochore is demonstrated in studies of cells with chromosomes lacking centromeres and thereby lacking kinetochores. In such studies chromosomes fail to segregate in anaphase and form micronuclei in telophase [23, 38, 48]. Micronuclei pose a significant threat to the cell as they can lead to the loss of genomic content [108], they are often sites of significant DNA damage [118], and they are a hallmark of cancer cells [8, 88].

Different types of acentrics

Acentric chromosome fragments can arise in mitosis through a variety of mechanisms. One such mechanism is the persistence of double-strand DNA breaks into mitosis. This leads to the formation of a kinetochore-bearing chromosome fragment with one telomeric end and one broken end and a chromosome fragment lacking a kinetochore, with one telomeric end and one

broken end (Figure 1.1A). The acentric chromosome fragment lacking a

kinetochore would be unable to make canonical attachments to the mitotic

spindle and are expected to be lost from the cell or form micronuclei.

Another well-known mechanism of creating acentric chromosome

fragments is via Robertsonian translocations. A Robertsonian translocation

occurs when two acrocentric chromosomes break at their centromeres and fuse

together to form a metacentric chromosome with two centromeres and a small

acentric fragment (Figure 1.1B). Similarly, induced recombination between sister

chromatids using FLP recombinase produces an acentric chromosome

containing two telomeric ends and a dicentric chromosome [102]. These

acentrics would also be unable to make canonical attachments to the mitotic

spindle and are expected to be lost from the cell or form micronuclei.

Lastly, acentrics can arise through gene amplification events commonly

observed in cancer cells, known as chromothripsis [118]. During the development

of tumors, gene amplification events result in the formation of small, circular

chromosome fragments lacking a centromere and telomeres, termed "double

minutes" (Figure 1.1C). Double minutes often lack regulatory elements allowing

genes to be continually expressed further contributing to gene amplification [73].

A Acentric fragment

Cause:
Endonuclease
X-ray irradiation
DSB break-inducing mutagen

Product:
Acentric with one broken end
and one telomere

B Double-telomere acentric

Cause:
Robertsonian translocation
Inverted repeats

Product:
Acentric with two telomeres

C Double minute

Cause:
Gene
amplification

Product:
Circular acentric
with no telomeres
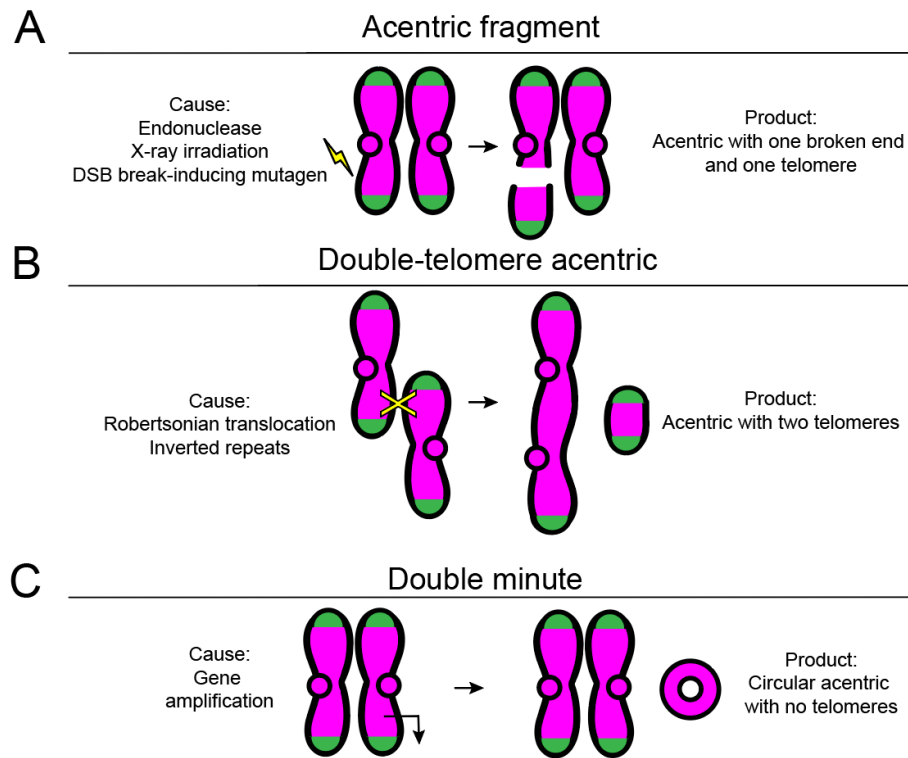
Figure 1.1: Schematic of different forms of acentric chromosomes.
(A) Acentrics generated via double-strand DNA breaks have one broken end and one telomere-capped end. (B) Acentrics generated via Robertsonian translocations or inverted repeats have two telomere-capped ends (referred to as "double-telomere acentrics"). (C) Acentrics generated via gene amplification are circular with no broken ends or telomere-capped ends (referred to as "double minutes").

Transmission of acentric chromosomes occurs in a variety of organisms

Successful transmission of chromosome fragments has been seen in a variety of cell types. Early evidence of acentric chromosome transmission was shown in grasshopper neuroblasts. Generated through X-ray irradiation, acentric chromosome fragments were positioned at the metaphase plate, lagged behind kinetochore-bearing chromosomes during anaphase, but segregated poleward and were either incorporated into the reforming daughter nuclei or formed

micronuclei [11]. In crane fly spermatocytes, laser microsurgery was used in metaphase to create acentric chromosome fragments which displayed poleward movement in anaphase [48]. Successful transmission of endonuclease-induced acentrics has also been reported in *Drosophila melanogaster* with around 95% of neuroblasts displaying poleward movement of acentrics in anaphase [85].

In addition to this work, acentric chromosome transmission has also been observed in *Schizosaccharomyces pombe* [35]. After conditional deletion of the centromere, a subset of the surviving cells contained acentric chromosome fragments indicating the transmission of acentrics through multiple cell cycles [35]. In *Saccharomyces cerevisiae,* endonuclease-induced acentrics demonstrate alignment at the metaphase plate and poleward segregation in anaphase [42]. In irradiated *Scadoxus multiflorus* cells, acentric chromosomes successfully aligned at the metaphase plate and moved poleward in anaphase [4].

Proper acentric chromosome transmission has also been reported in mammalian cells. In human cancer cells under selective pressure, double minutes persisted within cells over several cell divisions [73]. Live analysis of human cancer cell lines has also revealed transmission of double minutes to daughter cells [37]. In human lymphocytes, 60% of cells with lagging acentric fragments divided without forming micronuclei, suggesting successful incorporation of the acentrics into reforming daughter nuclei [20]. In *Potorous tridactylus* cells, 54% of acentrics generated by laser microsurgery demonstrated poleward movement during anaphase [69].

Taken together, these studies highlight the remarkable ability of acentric chromosomes to align at the metaphase plate, successfully separate and segregate in anaphase, and join the kinetochore-bearing chromosomes in the reforming daughter nuclei. The mechanisms by which acentrics are using to accomplish these feats remain poorly understood. Potential mechanisms include

neocentromere formation [78] and direct association of the acentric to a

kinetochore-bearing chromosome [35, 36, 65] or microtubules [40, 109].

Type of acentric chromosome	Organism	Proposed mechanism of transmission	References
"Acentric fragment"	*Drosophila melanogaster*	DNA tethers and microtubules	Royou et al., 2010; Karg et al., 2015; Bretscher and Fox, 2016; Karg et al., 2017; Warecki and Sullivan, 2018; Vicars et al., 2021
	Chortophaga vididifasciata		Carlson, 1938a
	Nephrotoma suturalis	DNA tethers and microtubules	LaFountain et al., 2001; LaFountain et al., 2002a
	Potorous tridactylus	DNA tethers	Ono et al., 2017
"Double-telomere acentric"	*Schizosaccharomyces pombe*	DNA tethers	Ishii et al., 2008; Ohno et al., 2016
	Drosophila melanogaster		Titen and Golic, 2008
	Pales ferruginea	Microtubules	Fuge, 1975
"Double minute acentric"	*Homo sapiens*	DNA tethers	Pauletti et al., 1990; Kanda et al., 1998; Falck et al., 2002
	Scadoxus multiflorus	Microtubules	Bajer, 1958; Bajer and Vantard, 1988; Khodjakov et al., 1996
	Saccharomyces cerevisiae	DNA tethers	Kaye et al., 2004

Table 1.1: Summary of examples of acentric transmission. Examples of
acentric transmission are organized by acentric type, the organism in which they
were observed, and the proposed transmission mechanism. Mechanisms were
left blank if unknown.

Mechanisms of acentric transmission

Despite being observed in a diversity of organisms, the transmission of

acentric chromosomes through cell division remains poorly understood. One

method by which acentrics could be transmitted is by directly interacting with a

kinetochore-bearing chromosome (Figure 1.2B). The acentric would then be able

to follow the kinetochore-bearing chromosome to the metaphase plate, past the

spindle equator, and to the appropriate cell pole. Several studies have revealed

direct attachments of acentrics to kinetochore-bearing chromosomes in many

different organisms.

In *Drosophila melanogaster*, DNA tethers containing histones and coated

in associated proteins (chromosomal passenger complex proteins Aurora B

kinase and INCENP, cell cycle kinases BubR1, Bub3, and Polo, and the APC/C

cofactor Cdc20) have been observed connecting acentrics to their centric

7

partners during mitosis [85]. Functional analyses of the tether-associated proteins reveal that these components are required for proper acentric alignment at metaphase and separation and segregation in anaphase. Disruptions in BubR1 and Polo function result in misalignment of the acentrics at metaphase and failure in acentric separation and segregation during anaphase [85]. This protein-coated DNA tether could be providing elastic force to facilitate the transport of acentrics to the metaphase plate and to opposing poles in anaphase (Figure 1.2B).

In fission yeast, acentrics with two telomeric ends have been observed to fuse with centromere-bearing chromosomes and be transmitted through subsequent cell cycles [35, 65]. In human cells, double minutes form clusters in anaphase and attach themselves to centromere-containing chromosomes. Consequently, the double minutes follow the centromere-containing chromosomes as they travel poleward [37] (Figure 1.2D). In *Drosophila* papillary cells, broken acentric chromosomes accurately align at metaphase and separate and segregate in anaphase over several cell division cycles [9].

Acentrics could also form connections with kinetochore-bearing chromosomes through DNA catenations. In *Allium cepa* cells, DNA catenations link acentric fragments together in metaphase [27]. In *Drosophila* larval neuroblasts, DNA catenations keep acentric fragments paired during anaphase [109]. Resolution of these catenations is achieved by Topoisomerase II activity and microtubule plus-end pushing forces [27, 109].

Although, the tether does not appear to be the only potential force acting on acentrics. Work in *Drosophila* has revealed acentrics with one telomere-capped end and one broken end tend to travel poleward with either their telomeres leading or telomeres lagging in roughly equal frequencies [40]. These results suggest connections between the broken end of the acentric and its

centric partner are not the only driving force for acentric transport in mitosis. Studies found the role of the tether is to incorporate the acentric fragment into the reforming daughter nuclei in telophase [41, 114]. However, the roles of DNA catenations and the centric-acentric tether in transporting acentrics poleward remain unclear. Although, these DNA connections between acentrics and kinetochore-bearing chromosomes could be allowing acentrics to maintain associations with the main mass of chromosomes and to interact with microtubules (Figure 1.2B).

In many systems, acentrics have been found to localize to the cell periphery in metaphase and anaphase [11, 40, 45, 47, 109]. This peripheral localization could be allowing the acentrics to interact with interpolar microtubules, either via lateral interactions or motor proteins (Figure 1.2B). Interestingly, disruptions in the chromokinesin Klp3A/KIF4 in *Drosophila* neuroblasts led to defective interpolar microtubule organization during cell division and an increase in acentric misalignment at metaphase and mis-segregation during anaphase [39, 40]. Microtubules have also been found to form bundles around acentric chromosomes in *Drosophila*, *Pales ferruginea*, and *Scadoxus multiflorus* [5, 25, 40, 44]. Additional experiments using the laser ablation of microtubules in anaphase uncovered an apparent physical connection between microtubules and the poleward traveling acentric [40]. Insight into the microtubule-associated proteins that could be facilitating these connections comes from studies done in *Drosophila* [109].

In *Drosophila*, the microtubule-stabilizing protein Map205 and the microtubule plus-end associated protein EB1 were found to be vital for effective separation of acentric sisters during anaphase [109]. Acentrics were found to predominantly separate from one another during anaphase via a lateral sliding mechanism potentially driven by lateral interactions with microtubules. Partial

knockdowns of EB1 or Map205 using RNAi disrupted this mode of acentric

separation [109]. Overall, microtubule stabilization and plus-end pushing forces

appear to be vital to the separation and segregation of acentric sister

chromosomes during anaphase. Still, the precise mechanisms by which acentrics

are interacting with the mitotic spindle have yet to be completely explored.
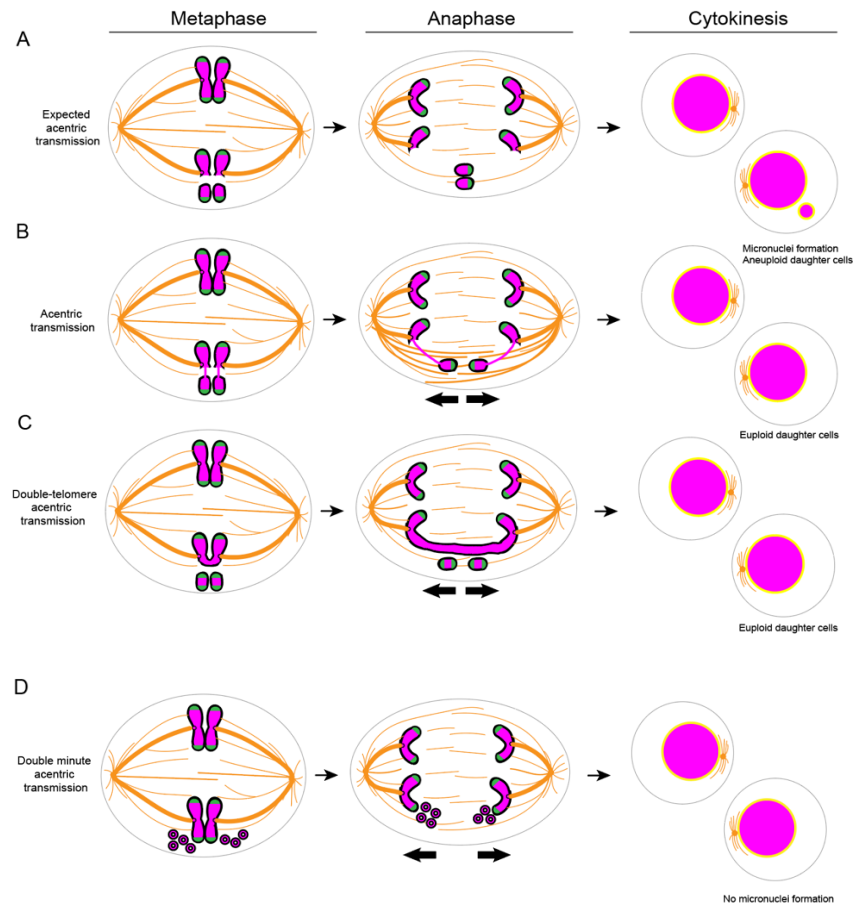
Figure 1.2: Schematic of acentric chromosome transmission mechanisms.
(A) Acentrics are expected to be unable to make canonical attachments to microtubules, lag behind in anaphase, fail to separate and segregate, and lead to the formation of micronuclei and aneuploid daughter cells. (B) Acentrics with one broken end and one telomere-capped end may align at the metaphase plate and separate and segregate poleward with the help of a DNA tether connecting it to its centric partner and microtubules. (C) Acentrics with two telomere-capped ends are able to separate and segregate poleward potentially due to DNA tethers or microtubule-based forces. (D) Double minutes are able to segregate in mitosis possibly by clustering and forming catenations with kinetochore-bearing chromosomes.

Conclusions and future perspectives

The work described above highlights how DNA tethers, microtubules, and associated proteins play important roles in acentric congression, separation, and segregation. However, further studies are needed to uncover the details behind these events. It remains unknown if there is an acentric specific motor protein guiding its transport, if acentrics are interacting with microtubules directly or with the help of microtubule-associated proteins, or if the DNA tether and associated proteins provide sufficient force to transport acentrics. Insight into these mechanisms can aid in our fundamental understanding of chromosome transmission.

In *Drosophila* neuroblasts and papillary cells, acentric sister chromosomes tend to lag behind during anaphase, but remarkably, eventually separate and segregate to opposing cell poles with high fidelity [9, 85]. Lacking kinetochores, it remains unclear how these acentrics are able to move to the appropriate cell pole with such high success rates [9, 85]. Explored mechanisms include connections between the acentric and its centric partner via a protein-coated DNA tether and lateral interactions between the acentric and microtubules [40, 85].

Additionally, the fate of acentrics after successful inclusion into daughter nuclei remains unknown. Since a high survival rate is seen in *Drosophila* after induction of broken acentric chromosomes throughout the organism, it is presumed that these acentric fragments are eventually repaired in subsequent cell cycles [85]. Alternatively, the presence of acentric chromosomes during cell division could trigger apoptosis [10, 64, 102] or lead to the formation of micronuclei [118]. Further investigation is required to determine how the cell copes with acentric chromosomes in subsequent cell division cycles.

Chapter 2: Kinetochore-independent mechanisms of sister chromosome separation

Abstract

Although kinetochores normally play a key role in sister chromatid separation and segregation, chromosome fragments lacking kinetochores (acentrics) can in some cases separate and segregate successfully. In *Drosophila* neuroblasts, acentric chromosomes undergo delayed, but otherwise normal sister separation, revealing the existence of kinetochore-independent mechanisms driving sister chromosome separation. Bulk cohesin removal from the acentric is not delayed, suggesting factors other than cohesin are responsible for the delay in acentric sister separation. In contrast to intact kinetochore-bearing chromosomes, we discovered that acentrics align parallel as well as perpendicular to the mitotic spindle. In addition, sister acentrics undergo unconventional patterns of separation. For example, rather than the simultaneous separation of sisters, acentrics oriented parallel to the spindle often slide past one another toward opposing poles. To identify the mechanisms driving acentric separation, we screened 117 RNAi gene knockdowns for synthetic lethality with acentric chromosome fragments. In addition to well-established DNA repair and checkpoint mutants, this candidate screen identified synthetic lethality with X-chromosome-derived acentric fragments in knockdowns of Greatwall (cell cycle kinase), EB1 (microtubule plus-end tracking protein), and Map205 (microtubule-stabilizing protein). Additional image-based screening revealed that reductions in Topoisomerase II levels disrupted sister acentric separation. Intriguingly, live imaging revealed that knockdowns of EB1, Map205, and Greatwall preferentially disrupted the sliding mode of sister acentric separation. Based on our analysis of EB1 localization and knockdown phenotypes, we propose that in the absence of a kinetochore, microtubule plus-

end dynamics provide the force to resolve DNA catenations required for sister separation.

Introduction

Eukaryotic cells have evolved mechanisms to detect and protect against genomic insults. These mechanisms include checkpoint pathways that delay cell cycle progression allowing time for repair as well as apoptotic pathways that eliminate the damaged cells from the dividing population [19]. Although a great deal is known regarding the function of these corrective pathways during interphase, much less is known about the mechanisms that protect against genomic instability after exit from metaphase. Studies demonstrate that DNA damage persisting through metaphase delays anaphase onset. This delay is mediated both by the DNA damage and spindle assembly checkpoint pathways [59, 86].

Despite these mechanisms, if the DNA damage remains, the checkpoints are overridden, and the cell exits metaphase [15]. The persistence of unrepaired double-strand breaks (DSBs) at metaphase is particularly problematic due to the formation of chromosome fragments, one of which lacks a telomere and the other lacking a kinetochore and a telomere. The latter type are known as acentrics and are incapable of forming canonical microtubule-kinetochore attachments that drive sister chromosome separation and segregation. Consequently, acentrics would be expected to lag on the metaphase plate and exhibit severe segregation defects. In accord with this expectation, acentrics often fail to segregate, are excluded from daughter nuclei, and subsequently form cytoplasmic micronuclei [23, 38, 48]. However, a growing number of reports demonstrate poleward migration of acentric chromosome fragments [4, 9, 37, 38, 85, 44, 50]. Proposed

mechanisms of acentric segregation include neo-centromere formation [78] and direct association of the acentric chromosome with microtubules [40] or a kinetochore-bearing chromosome [35, 36, 65].

Acentrics are efficiently induced in *Drosophila* bearing an I-CreI endonuclease transgene, which fortuitously recognizes a repetitive sequence within the pericentric rDNA repeats of the *Drosophila* X chromosome [28, 52, 71, 84]. Induction of I-CreI expression results in the formation of acentrics in over 80% of third instar larval neuroblast cells [85]. Although acentrics lag behind on the metaphase plate well after the intact chromosomes migrate toward opposite poles, the acentrics have a remarkable ability to accurately separate, segregate and incorporate into daughter telophase nuclei [115]. A previous study done in the lab found that acentric segregation relies on the chromokinesin Klp3A and interpolar microtubules [40]. However, it remains unclear how sister acentrics are held together on the metaphase plate well after the main chromosome mass has separated. Additionally, it is unknown how acentric sisters are able to initially separate from one another instead of segregating together poleward. These behaviors reveal the existence of kinetochore-independent mechanisms maintaining sister chromosome association on the metaphase plate and driving their separation during anaphase. Possible explanations include delayed acentric cohesin removal, delayed resolution of sister DNA catenations, or opposing plus-end directed microtubule forces acting on each sister. Here we employ a combination of synthetic lethal screens and live imaging to identify factors required for proper separation of sister acentrics. Live analysis reveals three distinct modes of acentric separation: unzipping, sliding, and simultaneous dissociation. This candidate screen revealed that Topoisomerase II, the cell-cycle regulator Greatwall kinase, the microtubule (MT) plus-end tracking protein EB1, and the MT-associated protein Map205 provide key roles in sister separation of

acentrics. In addition, gene knockdowns of EB1, Map205, and Greatwall preferentially disrupt the sliding mode of sister separation. As will be discussed, this analysis demonstrates the existence of kinetochore-independent mechanisms facilitating sister chromosome separation.

Results

Acentric sister separation, but not cohesin removal, is delayed during the metaphase-to-anaphase transition

As described previously, acentric chromosome fragments are efficiently generated through heat-shock induction of an I-CreI transgene that specifically targets and creates DSBs in the rDNA repeats at the base of the *Drosophila* X chromosome [84]. In accord with previous studies [85], live analysis of the resulting X chromosome acentrics in the larval neuroblasts reveals that sister separation of the acentrics occurs on average 148 seconds (± 44, N = 19) after separation of the intact chromosomes (Figure 2.1). We define acentric sister separation as the point in which the sister acentrics can be clearly distinguished. Acentric sister segregation is defined as the interval between separation of sisters and their migration to the spindle pole. The delay in timing of acentric separation is defined as the time elapsed between the initiation of intact sister chromosome separation and that of acentric sister separation. Sister chromatids are held together at metaphase by cohesin, a tripartite ring-like protein complex comprised of two structural maintenance of chromosome proteins (SMC1, SMC3) and a kleisin subunit (Rad21/Scc1) [30, 58]. Initially, cohesin removal occurs only along the chromosome arms through proteolytic cleavage of the kleisin subunit by separase just prior to anaphase onset [67, 104, 105]. Due to the Sgo/PP2A-dependent protection mechanism, cohesin remains at the

centromeric regions [31]. Once cohesin is removed, microtubules drive sister separation [3, 68].

To investigate if delays in cohesin release are responsible for the delayed separation of acentric chromosomes, female neuroblast divisions were live imaged with a cohesin component, Rad21, tagged with EGFP [106]. Time-lapse images of a control neuroblast expressing Rad21-EGFP are shown in Figure 2.2A (chromosomes in magenta, cohesin in green). No lagging chromosomes are observed and Rad21 is cleared off of all chromosomes just prior to anaphase onset and separation of sister chromatids. Figure 2.2B and Table S2.1 data show time-lapse images of an I-CreI-expressing neuroblast division. Separation and segregation of sister acentrics is delayed relative to the intact chromosomes. Interestingly, cohesin removal just prior to anaphase onset from the acentrics and the intact kinetochore-bearing chromosomes occurs simultaneously. This is more clearly seen in the single channel black and white cohesin images of Figure 2.2B (depicting yellow outlined regions of Figure 2.2B). Quantification of the Rad21 fluorescent signal supports the conclusion of a relatively synchronous removal of cohesin on the acentric and intact chromosomes (Figure 2.2C). The finding that sister acentrics remain paired despite the absence of cohesin and well after the intact chromosomes have separated, indicate additional forces must hold sister acentrics together.
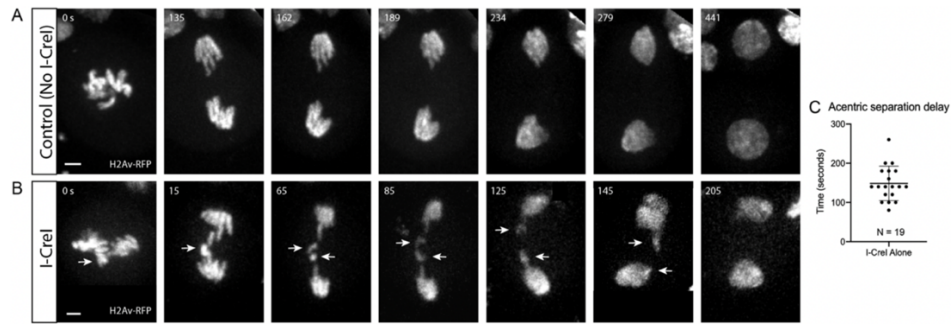
Figure 2.1: Acentric sister separation is delayed relative to kinetochore-bearing chromosomes during anaphase. (A) Still frames of a time-lapse movie of a mitotic neuroblast labeled with H2Av-RFP and not expressing I-CreI. (B) Still frames of a time-lapse movie of a mitotic neuroblast with I-CreI induced acentrics. Separation of sister acentrics (arrows) is delayed. Consequently, they lag on the spindle equator but eventually separate, segregate, and are reincorporated into daughter nuclei. Bars, 2 μm. Time in seconds. (C) Scatterplot showing the delay in acentric sister separation after anaphase onset. Delay (seconds) was measured from when kinetochore-bearing chromosomes initiated separation to when acentric sister chromosomes initiated separation. Bars represent mean and standard deviations.
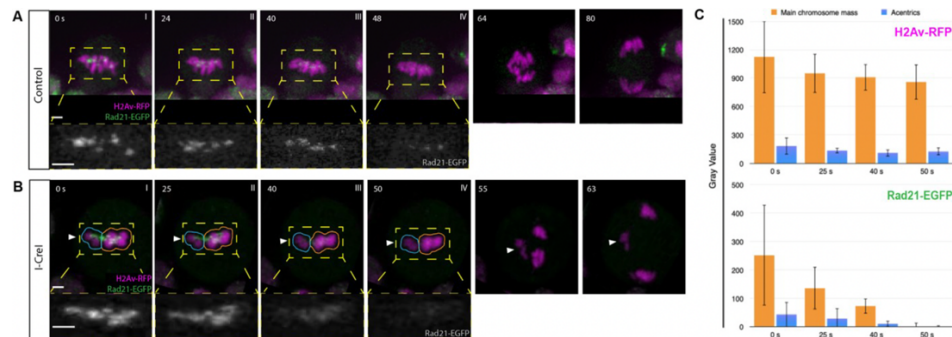
Figure 2.2: Cohesin complexes are cleared off of acentric sisters upon anaphase onset. Chromosomes labeled with H2Av-RFP (magenta) and cohesin labeled with Rad21-EGFP (green). (A) Stills from a time- lapse movie of a control mitotic neuroblast. (B) Still images from a timelapse movie of a mitotic neuroblast with I-CreI-induced acentrics. Acentrics (arrowhead) lag on the spindle equator. (C) Bar graphs of a compilation of five videos of I-CreI- expressing neuroblasts showing the relative fluorescence intensities in arbitrary units (AU) of chromosomes (H2Av-RFP, top) cohesin (Rad21-EGFP, bottom) around acentrics (cyan outlined region) and the main mass of chromosomes (yellow outlined region) at time points 50, 40, 25, 0 s, prior to anaphase onset, respectively. Bars, 2 μm. Time in seconds. Error bars represent standard deviations of fluorescence intensities at all points tested.

Acentric sister separation occurs via three distinct patterns

To examine dynamics of acentric separation, we imaged live neuroblasts expressing I-CreI, the histone marker H2Av-RFP, and the telomere marker HOAP-GFP [12]. Marked telomeres enabled us to determine the orientation of acentrics with respect to one another as they aligned on the metaphase plate, separated, and segregated poleward [40]. We observed three distinct patterns of sister acentric separation (Figure 2.3). In the most frequent pattern (49%, N = 45), acentric pairs separate by sliding past one another (Figure 2.3A, Top row: histone-labeled chromosomes in magenta, HOAP-labeled telomeres in green). This is more clearly observed in the single histone channel movie (Figure 2.3A Bottom row and Table S2.2). Also, in contrast to intact kinetochore-bearing chromosomes which always align perpendicular to the spindle, the paired sister acentrics align either parallel or perpendicular to the spindle and division axis.

The second pattern of acentric separation occurs via an "unzipping" mechanism (Figure 2.3B). This pattern occurs at a frequency of 31% (N = 45). During separation, sister acentrics often first separate at the broken end followed by separation at the telomere. This is illustrated in Figure 2.3B: the telomeres remain associated while the broken ends are well separated. Rarely, the paired acentrics unzip from the telomere end first. In contrast to the acentrics that separate by sliding, these paired sister acentrics are frequently aligned perpendicular to the spindle and division axis.

In the third pattern of separation, the remaining 20% (N = 45), acentric sisters cleanly separate from one another along their entire length similar to that observed for centric chromosomes (Figure 2.3C). We termed this centric-like pattern: simultaneous dissociation. Acentrics that separate via simultaneous dissociation are aligned in multiple orientations on the metaphase plate (from

18

parallel to perpendicular) with respect to the spindle and division axis. At separation, dissociating sister acentrics simultaneously separate along their entire lengths.

We next analyzed the orientation of sister acentrics with respect to one another at the time of separation through labeling telomeres with HOAP-GFP. As expected, the vast majority (87%, 39/45) of sister acentrics were oriented with their telomeres paired and aligned (Figure 2.3D). However, a small but notable fraction (13%, 6/45), aligned with their telomeres opposed (Figure 2.3D). Acentric pairs that align with telomeres opposed presumably have already lost catenation and/or cohesin in order to adopt this geometry. 14% and 33% of acentric sisters that separated by sliding and dissociating, respectively, aligned with their telomeres opposed. Interestingly, sister acentrics that separated by unzipping were never observed aligned with their telomeres opposed. This suggests that there is an absolute requirement for sister pairing in acentrics that separate by unzipping.

To further characterize these three modes of acentric separation, we measured the time from anaphase onset (as determined by separation of the intact chromosomes) to sister acentric separation (Figure 2.3E). Sliding acentrics separated much later than acentrics (202 ± 51 seconds) that separated either by unzipping (131 ± 54 seconds) or dissociating (106 ± 55 seconds) (N = 45, Figure 2.3E). These differences were statistically significant as determined by two-sided Mann-Whitney tests (P = 0.0008 and P = 0.0008, respectively). We did not detect any difference in the timing of acentric sister separation by unzipping or dissociating (P = 0.25 as determined by a two-sided Mann-Whitney test).

Taken together, these results demonstrate three distinct patterns for acentric separation. We note that based on the movements and orientation of both sliding and dissociating acentrics, it is possible that catenations are lost

19

along the entire length of the acentric pair simultaneously at the moment of

separation. In contrast, acentrics that separate by unzipping and appear to have

an absolute requirement for sister pairing may be more tightly associated with

one another, and this tight association may be due to lingering catenations.
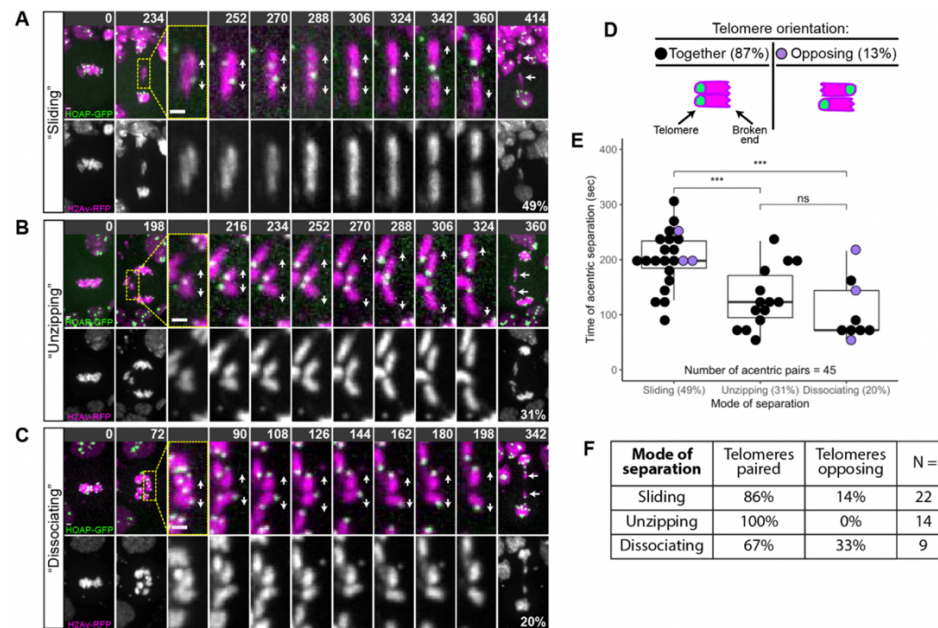
Figure 2.3: Sister acentrics separate via three distinct patterns.
Chromosomes labeled with H2Av-RFP (magenta) and telomeres labeled with
HOAP-GFP (green). Telomeres indicated by yellow arrowheads. Direction of
separation indicated by white arrows. (A) Top row: Still images of a time-lapse
movie of a mitotic neuroblast with I-CreI induced acentrics showing sister
acentrics (cyan arrows) lagging behind during anaphase, paired with telomeres
opposing, sliding past one another, and ultimately separating. Bottom row: Black
and white images of sister acentrics sliding past one another (see arrows). (B)
Top row: Still images of a time-lapse movie of a mitotic neuroblast with I-CreI
induced acentrics showing acentrics (cyan arrows) lagging on the metaphase
plate. In a process we term "unzipping", sister acentrics are aligned with
telomeres paired, initiate separation at their broken ends followed by separation
of telomeres. Bottom row: Black and white images of sister acentrics unzipping
(see arrows). (C) Top row: Still images of a time- lapse movie of a mitotic
neuroblast with I-CreI induced acentrics showing sister acentrics (cyan arrows)
lagging behind during anaphase. In a process we term "simultaneous
dissociation", sister acentrics simultaneously separate along their entire length.
Bottom row: Black and white images of sister acentrics simultaneously
separating along their entire lengths (see arrows). (D) Frequency of acentric
sisters paired with their telomeres aligned or in opposite orientations. (E)
Measurements of the frequency of each mode of acentric sister separation (x-

axis) and the timing of acentric sister separation after intact chromosomes separate (y-axis). Each dot represents on acentric pair. Black dots represent acentric sisters with telomeres aligned and purple dots represent acentric sisters with telomeres oriented in opposite directions. Boxes show interquartile ranges and lines show medians of the measured data. Asterisks represent statistical significance (***P = 0.0008) determined by two-sided Mann-Whitney tests. (F) Chart showing the distribution of telomere orientations within each mode of acentric sister separation. Acentrics that separate by unzipping are always oriented with their telomeres paired.

Synthetic lethal screen identifies genes required for separation of sister acentrics

To identify the mechanisms required for transmission of acentric sister chromosomes, we screened candidate RNAi gene knockdowns that resulted in synthetic lethality in the presence of acentrics. The rationale for this screen is based on previous studies demonstrating that I-CreI induction of acentric chromosomes during third instar larval stage resulted in only slight reductions in adult survival because the acentrics are efficiently transmitted to daughter nuclei [85]. However, reducing or partially disrupting the function of genes required for the normal acentric transmission results in a dramatic reduction in adult survival upon acentric induction [40, 85]. Thus, we expected that a subset of the gene knockdowns that resulted in synthetic lethality upon I-CreI induction would be required for proper pairing and segregation of sister acentrics.

To perform the screen, adult flies bearing a heat-shock inducible I-CreI endonuclease and Gal4 under the control of a ubiquitously expressed Actin enhancer element (Act5) were crossed to adults bearing UAS-gene specific RNAi constructs. Lethality of heat-shocked (I-CreI induced) and non-heat-shocked (I-CreI not induced) F1 progeny bearing both constructs were assayed. RNAi constructs that significantly increased lethality upon I-CreI induction were of particular interest. We screened 117 candidate genes for synthetic lethality upon acentric induction (Table S2.1). These included genes encoding proteins

21

spanning a diversity of mitotic functions, including microtubule-associated proteins, chromatin remodelers, DNA repair genes, cell cycle kinases, and cell cycle checkpoints. For each RNAi line, we determined the survival ratio of the RNAi knockdown with I-CreI induced to the RNAi knockdown alone (RNAi knockdown + I-CreI/RNAi knockdown) (Table 2.1). Because these RNAi knockdowns do not cause complete lethality, we classified hits as having a survival ratio of 65% or less (Table 2.1).

The acentrics are generated through I-CreI induced double-strand breaks. As expected, RNAi knockdowns of DNA repair and cell cycle checkpoints exhibit synthetic lethality upon I-CreI induction. Genes involved in DNA repair all exhibit strong synthetic lethality upon I-CreI induction. DSB repair genes *spnA/rad51* [94], *mus309* [56] and NHEJ gene *ku80* [57] exhibited survival ratios of 2%, 11%, and 29%, respectively (Table 2.1). The DNA damage checkpoint gene *tefu* (ATM [66]) also results in a pronounced synthetic lethality (survival ratio of 43%). The screen also yielded a number of microtubule-associated proteins. These included *msps* (microtubule nucleation [60]), *asp* (astral microtubule organization [89]), *eb1* (plus-end microtubule binding [81]), *klp68D* (kinesin motor protein [75]), and *map205* (microtubule stabilizer [2]). Given that microtubule-based transport plays a key role in the poleward transport of the acentric chromosome fragments [40], synthetic lethal interactions with microtubule-associated proteins were expected. However, it was unclear whether microtubules and their associated proteins also play a role in the initial separation of sister acentrics during the metaphase-to-anaphase transition. The screen also yielded a large class of genes involved in chromatin organization. Synthetic lethal interactions with chromatin organizing proteins were expected due to the presence of I-CreI induced DSBs. This included *cap-D2* (condensin [90]), *chd1* (ATP-dependent chromatin remodeler [95]), *sin3A* and *sir2* (histone deacetylases

[22]), *chrac* (nucleosome mobilization [14]), and *hp1* (heterochromatin protein [18]). Whether these are directly required for double-strand break repair, separation and/or segregation of sister acentrics remains to be determined. In accord with previous work, reduced levels of BubR1 kinase (spindle-assembly checkpoint protein) also exhibited a pronounced synthetic lethality upon I-CreI induction [85]. The screen also yielded two additional cell cycle kinases: *gwl* (greatwall kinase, an inhibitor of the cell cycle phosphatase PP2A [117]) and *ald* (altered disjunction, chromosome segregation [70]). We chose to focus on EB1 and Map205 due to their well-documented association with microtubules [2, 81]. Greatwall was chosen for follow-up because previous studies demonstrated that this kinase is required for sister separation of intact chromosomes [111].

	Gene RNAi	Survival rate with RNAi and I-CreI induced / Only RNAi induced	Rate of larvae-to-adult survival of RNAi with I-CreI induction % ± SD (N)	Rate of larvae-to-adult survival of RNAi without I-CreI induction % ± SD (N)
	Wildtype (Control)	88%	80 ± 21 (194)	91 ± 7 (194)
Chromatin-associated:	*hyx* (2)	10.0%	8 (25)	88 (25)
	cap-D2	12%	6 (17)	50 (12)
	chd1	30.0%	10 ± 17 (69)	33 ± 6 (99)
	sin3A	33%	8 (25)	24 (25)
	chrac-14 (2)	48%	48 (25)	100 (25)
	chd1 (2)	50.0%	48 (25)	95 (23)
	spt4	55%	24 (25)	44 (25)
	sir2	60.0%	64 (25)	94 (16)
	hp1e	65%	65 (20)	100 (25)
Microtubule-associated:	*msps*	27%	18 ± 17 (56)	67 ± 24 (30)
	asp (2)	46%	44 (25)	96 (25)
	EB1	47%	44 ± 25 (86)	94 ± 9 (38)
	Klp68D	51%	29 (24)	57 (21)
	asp	52%	52 (25)	100 (15)
	map205	65%	54 ± 18 (141)	83 ± 13 (91)
DNA repair/checkpoint:	*spnA*	2%	2 ± 4 (57)	82 ± 18 (99)
	mus309	11%	10 ± 1 (42)	95 (22)
	ku80	29%	28 (25)	96 (25)
	tefu	43%	43 (30)	100 (25)
	cp190	48%	12 (17)	25 (12)
Cell cycle kinase:	*bubR1*	3%	1 ± 2 (168)	31 ± 23 (69)
	gwl (2)	8%	2 ± 2 (112)	26 ± 10 (99)
	ald	59%	52 (25)	88 (25)

Table 2.1: Top hits from synthetic lethality screen. Top hits from the synthetic lethality screen were grouped by gene function. Overall survival rate ratio was determined by the following: (percentage of surviving larvae after RNAi and I-CreI induction) / (percentage of surviving larvae after only RNAi induction). Those RNAi transgenes that resulted in significant reduction in survival (a ratio of less than 0.65) were considered for follow-up live analysis.

Live imaging analysis reveals the microtubule-associated proteins Map205 and EB1 and Topo II are required for separation, but not segregation of sister acentrics

We conducted live imaging experiments on neuroblasts to investigate the effect of specific RNAi-mediated gene knockdowns on acentric mitotic transmission. Each line contains an RFP- tagged histone transgene facilitating live confocal analysis [91]. Based on previous studies revealing the role of microtubules in acentric transmission [40], we initially focused on the microtubule-stabilizing protein Map205 and the microtubule plus-end associated protein EB1.

In a wild-type background, the majority of acentrics line up at the outer edge of the metaphase plate, separated from the main mass of intact chromosomes [40, 85]. As described above and in previous publications, during anaphase sister acentrics remain paired on the metaphase plate well after the separation of intact chromosomes (Figure 2.4A) [40, 85]. On average, separation of sister acentrics occurs 148 seconds ± 44 (N = 19) after separation of the kinetochore-bearing chromosomes (Table 2.2). 83% (19/23) of acentric sister chromatid pairs separate normally with sister acentrics going to opposite cell poles (Figure 2.4C). In the remaining 17% (4/23), acentric sister chromatids line up in metaphase, lag behind at the metaphase plate, and segregate together to one pole of the cell (Table 2.3). Micronuclei form in telophase in 24% (4/17) of neuroblasts expressing I-CreI micronuclei form in telophase (Figure 2.4D).

Live imaging of acentric behavior in neuroblasts expressing Map205 RNAi revealed that 46% (10/22) of acentric sister chromatids do not separate from one another and segregate to one cell pole together, in comparison to 17% (4/23) in a wild-type background (Figures 2.4C and 2.5B and Table 2.3).

Additionally, after partial knockdown of Map205, sister acentrics separated from one another significantly earlier than acentrics in a wild-type background (P = 0.001, Mann-Whitney test, Table 2.2). In spite of defects in acentric sister chromatid separation, their average poleward segregation velocity was normal (Table 2.4). Despite the increase in failed acentric separation, there was not an increase in micronuclei formation (21% compared to 24% in controls) (Figure 2.4D).

Live analysis of acentric behavior in neuroblasts expressing EB1 RNAi revealed that 47% (14/30) of acentric sister pairs fail to separate (Figures 2.4C and 2.5E and Table 2.3). The failure of separation results in acentric sisters segregating together to a single cell pole (Figure 2.4B). Additionally, the delay in acentric separation and their rate of poleward segregation were normal (Figure 2.5E and Tables 2.2 and 2.4). There was also not an increase in micronuclei formation (15% compared to 24% in controls) (Figure 2.4D). This indicates that the Map205 and EB1 knockdowns are specifically disrupting sister separation of acentrics and have no effect on the latter stages of acentric transmission.

As described earlier, cohesin removal on the intact chromosomes and acentrics occurs simultaneously, yet acentric sisters remain paired. This raised the possibility of a role for DNA catenation in maintaining acentric pairing. Previous work demonstrated that DNA catenations preserve sister chromatid cohesion in intact chromosomes until resolution by Topoisomerase II (Topo II) at the metaphase-anaphase transition [79]. Topo II decatenates intertwined DNA allowing sister chromatids to segregate to opposing poles of the cell. To test the role of DNA catenation in maintaining acentric sister pairing, we knocked down levels of Topo II specifically in the *Drosophila* neuroblast using the Gal4/UAS RNAi technique described above. Topo II knockdowns revealed that 54% (12/22) of sister acentrics fail to separate and subsequently segregate together to one

pole (Figure 2.6 and Table 2.3). Due to the lasting catenations between acentric

sisters, the initiation of acentric separation was further delayed in neuroblasts

expressing Topo II RNAi (Mann-Whitney test; P = 0.003) (Table 2.2). Although

acentric separation is disrupted, their poleward segregation rate and their rate of

micronuclei formation were normal (Figures 2.4D and 2.5F and Table 2.4).

The screen also yielded the PP2A inhibitor Greatwall kinase (*gwl*) that

controls the timing and events of mitotic exit including sister chromatid separation

[111]. Thus, we were particularly interested in the dynamics of acentric

separation and segregation when the levels of *gwl* were reduced. This analysis

uncovered that with reduced levels of *gwl*, 39% (14/36) of acentric sister pairs

failed to separate from one another (Figures 2.4C and 2.5B and Table 2.3).

Additionally, the delay in acentric separation and the rate of micronuclei

formation were normal (Figures 2.4D and 2.5G and Table 2.2). However, the

average velocity of acentrics while segregating during anaphase was significantly

slower in *gwl* mutant background compared to acentrics in wild-type background

(P = 0.006; Mann-Whitney test) (Table 2.4).
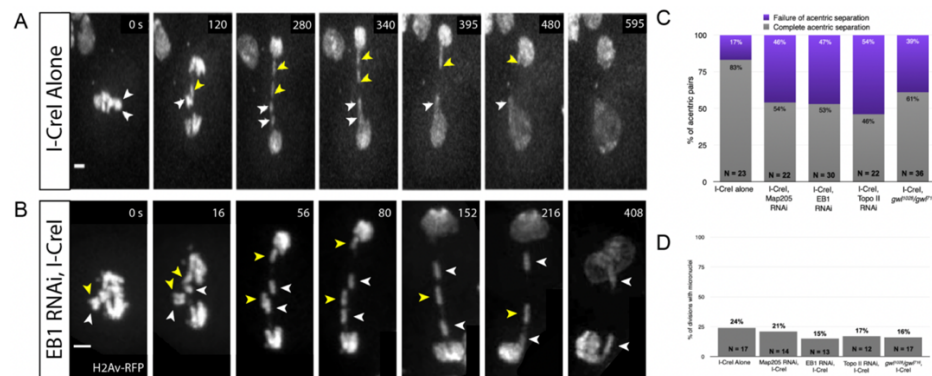
Figure 2.4: EB1 RNAi knockdowns specifically disrupt acentric sister separation. (A) Still frames of a time- lapse movie of a mitotic neuroblast with I-CreI induced acentrics. Paired sister acentrics (white and yellow arrowheads) lag behind at the spindle equator but eventually separate, segregate, and are reincorporated into daughter nuclei. (B) Still frames of a time-lapse movie of a mitotic neuroblast with I-CreI induced acentrics and expressing EB1 RNAi. Separation of paired sister acentrics (white and yellow arrowheads) fails,

26

resulting in sisters segregating to and incorporating into the same daughter nucleus. Bars, 2 µm. Time in seconds. (Video 3) (C) Percentages of neuroblast divisions in which acentric sisters failed to completely separate from one another. (D) Percentages of neuroblast divisions in which acentrics failed to incorporate into daughter nuclei and formed one or more micronuclei.

	Avg ± SD (seconds)	N (acentric pairs)
Control	148 ± 44	19
MAP205 RNAi	97 ± 39 **	12
EB1 RNAi	142 ± 57	16
Topo II RNAi	226 ± 77 *	10
gwl^{1028}/gwl^{716}	138 ± 49	22

Table 2.2: Sister separation of acentrics is delayed relative to sister separation of intact chromosomes. Average time (in seconds) for sister acentrics to initiate separation after sister kinetochore-bearing chromosomes separated. Time (average ± SD) measured from initiation of intact chromosome separation to initiation of acentric sister chromosome separation. Asterisks indicate statistical significance (**$P = 0.001$, *$P = 0.003$) as determined by two-sided Mann-Whitney tests.

	Fails to separate	Dissociate	Slides Apart	Unzip	N (acentric pairs)
Control	17%	13%	48%	22%	23
MAP205 RNAi	46%	9%	9%	36%	22
EB1 RNAi	47%	20.0%	13%	20.0%	30
Topo II RNAi	54%	14%	27%	5%	22
gwl^{1028}/gwl^{716}	39%	11%	28%	22%	36

Table 2.3: Acentric separation occurs through three distinct modes. Acentric sister chromatids either fail to separate or separate from one another by three different modes: laterally sliding past one another, unzipping from one another, or simultaneously and evenly dissociating along their lengths.
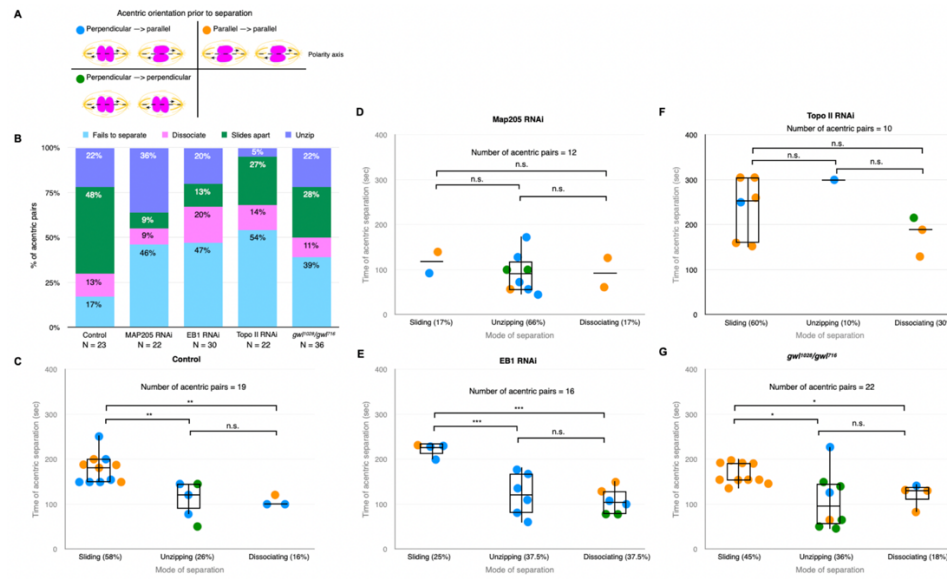
Figure 2.5: Knockdowns of EB1 and Map205 preferentially disrupt the sliding mode of acentric separation. (A) Model of different acentric orientations prior to separation. Polarity axis indicated by the dotted line. (B) Bar graph showing the percentage of acentric pairs that separate via simultaneous dissociation, sliding, or unzipping and the percentage of those that fail to separate. (C-G) Measurements of the frequency of each mode of acentric sister separation (x-axis) and the timing of acentric sister separation after the separation of intact chromosomes (y-axis). Each dot represents one acentric pair. Blue dots represent acentric pairs that were oriented perpendicular then parallel to the polarity axis prior to separation. Orange dots represent acentric pairs that were oriented parallel to the polarity axis prior to separation. Green dots represent acentric pairs that were oriented perpendicular to the polarity axis prior to separation. Boxes show interquartile ranges and lines show medians of the measured data. Asterisks indicate statistical significance (*P = 0.01, **P = 0.005, ***P = 0.009) when comparing the timing of acentric separation between separation modes. Statistical analysis was done using two-sided Mann-Whitney tests. Non-significant values had a P-value greater than 0.05.

	Avg velocity ± SD (nm/s)	N (individual acentrics)
Control	10 ± 4	26
MAP205 RNAi	12 ± 5	30
EB1 RNAi	10 ± 4	27
Topo II RNAi	12 ± 3	26
gwl^{1028}/gwl^{716}	8 ± 4 *	32

Table 2.4: Average velocities of acentric segregation. Depicted below are the velocities of individual acentrics as they segregate during anaphase. Velocity is measured in nanometers per second. Segregation velocity is defined as beginning when an acentric is clearly observed as separated from its sister and ends when the acentric reaches the daughter nucleus. Asterisks indicate statistical significance (*P = 0.006) as determined by a two-sided Mann-Whitney test.

EB1, Map205, Greatwall, and Topo II differentially influence the dynamics of acentric separation

As described above, in a wild-type background acentrics exhibit three distinct patterns of separation: sliding, unzipping, and simultaneous dissociation. Sliding is the most frequent occurring 49% of the time, with unzipping and simultaneous dissociation occurring at frequencies of 31% and 20%, respectively (Figure 2.3E). To determine the role of the genes identified above in these distinct forms of acentric separation, we monitored the frequency of segregation patterns in RNAi knockdowns of the candidate genes. Of those sister acentrics that successfully separated, knockdowns of Map205, EB1, and Greatwall resulted in a decreased frequency of separation via sliding (17%, 25%, 45%, respectively) compared to the control (58%) (Figure 2.5). Additionally, Topoisomerase II resulted in a decreased the frequency of acentric separation via unzipping (10%) compared to the control (26%) (Figure 2.5).

To determine if microtubule plus-ends preferentially accumulate around acentrics, I-CreI-expressing neuroblasts were live imaged with EGFP-tagged EB1. Fluorescence intensities of both GFP and RFP were measured and corrected for brightness in control neuroblasts (N = 5) and I- CreI-expressing neuroblasts (N = 5). During mitosis, EB1 localizes along microtubules moving towards the plus-ends (Figure 2.7). Previous studies have shown that EB1 is essential for generating antipolar forces on chromosomes [101, 110]. That finding together with our finding that EB1 is required for sister acentric separation motivated us to examine EB1 localization on the acentrics (Figure 2.7). We find the concentration of EB1 is not significantly increased on or near the acentrics (P > 0.05, two sample t-test; Figure 2.7). Thus, while EB1 and the acentrics co-localize, the pattern of EB1 comets is not altered in the presence of acentrics.

While these data are consistent with a role for EB1 in acentric sister separation, there is not an increase in recruitment and accumulation of EB1 at the acentric.
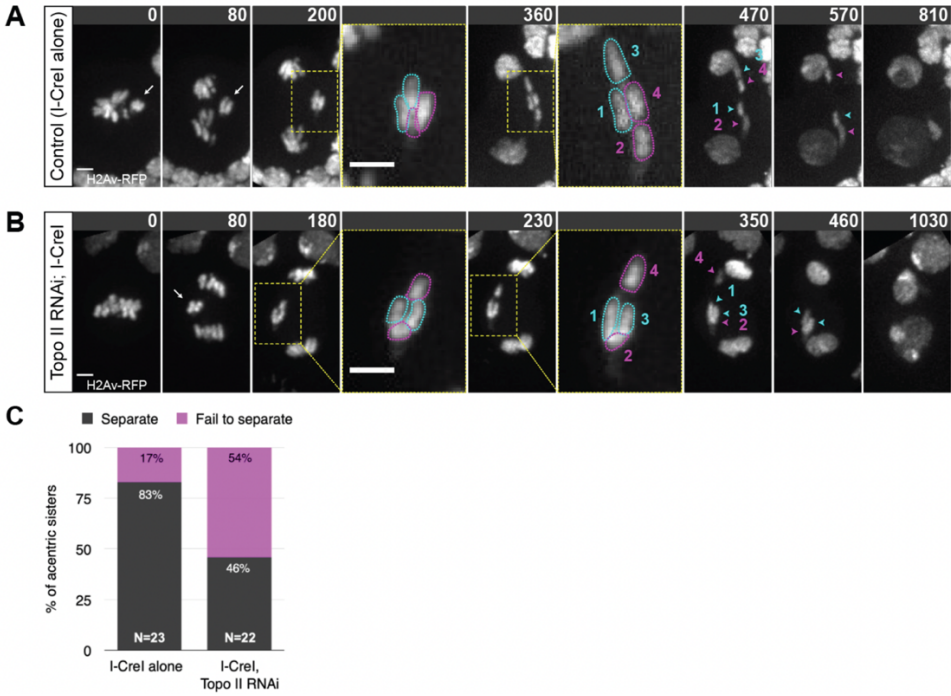
Figure 2.6: Acentrics appear to be held together by DNA catenations. (A) Still images of a time- lapse movie of a control neuroblast with I-CreI induced acentrics showing sister acentrics associated in early anaphase (white arrows), lagging behind and ultimately separating and segregating to opposite poles (cyan and magenta arrowheads). (B) Still images of a time-lapse movie of a neuroblast with partial knockdown of Topoisomerase II using RNAi and I-CreI induced acentrics. Acentrics associate and lag behind in early anaphase (white arrow), then fail to completely separate and segregate unequally (cyan and magenta arrowheads). Bars, 2 μm. Time in seconds. (C) Bar graph showing the quantification of acentric behavior in control and Topo II RNAi neuroblasts with the failure of acentric sister separation in magenta and the successful, even separation of acentric sisters in gray.

Discussion

These studies are based on the unexpected finding that sister chromosome fragments lacking a kinetochore undergo relatively normal separation. We sought to identify the kinetochore independent forces driving acentric sister chromatid separation. A key finding is that while cohesin removal occurs simultaneously on intact and acentric chromosomes, sister separation of the latter is significantly delayed. An explanation for this delay comes from studies of intact chromosomes demonstrating that once cohesin is removed, sister acentrics remain held together through DNA catenations [61, 79, 103]. Catenations are concentrated at the centromeric DNA and opposing kinetochore microtubule interactions likely provide the resolving force [7, 21, 43, 77, 112]. Support for this conclusion comes from studies of chromosome rearrangements in which centromeric heterochromatin is displaced from the centromere [68]. Sister chromatin separation is specifically delayed in these regions resulting in localized stretching during anaphase. A likely consequence of being displaced from the centromere is that the ectopic heterochromatic regions no longer experience sufficient kinetochore forces required to efficiently resolve sister DNA catenations. In light of these studies, it is likely that acentric sisters remain associated well after separation of the intact chromosomes through DNA catenations. This conclusion is supported by our finding that reductions in the Topoisomerase II levels specifically disrupt acentric sister separation. As described below, our studies suggest both plus-end and lateral microtubule interactions with the acentrics provide the alternative force driving sister separation.

Intact chromosomes align perpendicular to the spindle. In contrast, we find acentric chromosomes align either perpendicular or parallel to the spindle.

When aligned parallel to the spindle, acentrics travel with one tip leading towards the cell pole, possibly due to microtubule lateral interactions with acentrics. Without a kinetochore, a combination of lateral and plus-end microtubule interactions likely determines the final orientation of acentrics on the metaphase plate. In addition to the multiple orientations, acentrics undergo distinct patterns of sister separation that we have termed sliding, unzipping and simultaneous dissociation. Sliding of sisters past one another toward opposite poles is the most common mode of acentric separation. This mode occurs primarily when sister acentrics are oriented parallel to the spindle just prior to separation suggesting lateral microtubule interactions provide the force driving this mode of acentric separation (Figures 2.3A and 2.5C). While sister separation of all acentrics is delayed relative to intact chromosomes, the delay is much more pronounced for acentrics that undergo separation by sliding. The delay may in part be due to the additional time it takes to establish the multiple lateral interactions required to generate sufficient separation force. It is likely chromokinesins provide the force driving separation, but these have yet to be identified.

In contrast to sliding, sister separation by unzipping occurs primarily when the acentrics are oriented perpendicular to the spindle just prior to separation suggesting a limited role for lateral microtubule interactions (Figures 2.3B and 2.5C). During unzipping, acentrics generally initiate separation at their broken ends with completion of separation occurring at the telomeres. The delay of acentric separation by unzipping is much less than the delay observed for separation by sliding. Previous studies demonstrated that the acentric and its centric partner are connected via a DNA tether [85]. The preference for initiation of separation at the broken ends suggests that a DNA tether connecting the broken end to the kinetochore-bearing fragment may provide the initial separation force (Figure 2.3B). While this tether is not thought to provide the

force driving acentric segregation [40], because of its association with the broken end of the acentric, it may drive the initial stage of unzipping. In contrast to separation by sliding, telomeres are always aligned in sisters that separate by unzipping (Figures 2.3E and 2.3F). This suggests maintaining gene-for-gene sister pairing is essential for this form of separation.

The third mode of acentric separation, simultaneous dissociation, is characterized by a synchronized separation along the entire length of sister acentrics (Figure 2.3C). While sister separation via simultaneous dissociation favors the perpendicular orientation, this bias is much less dramatic compared to the unzipping mode (Figure 2.5C). The most distinguishing feature of this form of separation is the high frequency in which sister acentrics aligned with their telomeres opposed (33% compared to 14% and 0% for sliding and unzipping separation, respectively) (Figure 2.3F). This high frequency of unaligned telomeres suggests weak connections between sisters and that sister pairing is not required.

Synthetic lethal screens have proven an effective means of identifying factors required for the successful mitotic transmission of acentric chromosome fragments [40, 85]. These screens have identified proteins required for poleward transmission and final incorporation of acentrics into the telophase nucleus. Here we focused on identifying genes required for successful separation of sister acentrics. Of the 117 candidate genes screened, we identified 23 RNAi knockdowns/mutations that resulted in a significant lethality upon acentric induction (Table 2.1). Live analysis secondary screening revealed knockdowns of EB1 and Map205, and the cell cycle kinase Greatwall resulted in dramatic defects in acentric sister separation. Live imaging also revealed reducing levels of Topoisomerase II severely disrupted sister acentric separation.

Given that previous studies demonstrated the chromokinesin Klp3A is required for acentric poleward transport [40], it is not surprising that microtubule-associated proteins also play a key role in separation of acentric sisters. Reduced levels of EB1 and Map205 greatly increase the frequency of failed sister separation. EB1 is a plus-end tracking protein that associates with a number of regulatory proteins and is essential for generating anti-polar forces on the chromosomes [63]. EB1 knockdowns most dramatically reduce the frequency of acentric separation via sliding. In addition, for those acentric sisters that did separate by sliding in EB1 knockdowns, separation was greatly delayed. As lateral interactions between the microtubules and chromatin are likely to drive sister separation by sliding, we suspect plus-end directed EB1 forces may play a role in orienting the acentric in order to establish lateral interactions. Support for this idea comes from the finding of a synthetic lethal interaction between I-CreI induction and reductions in the levels of Nod, a non-motile chromokinesin that associates with EB1 and is involved in chromosome segregation [1, 40, 100, 116]. Surprisingly, a previous study in our lab found no effect on acentric segregation in mutations in *nod* [40]. Examining movies from this analysis revealed no significant difference in acentric sister separation in a loss-of-function *nod* mutant compared to the control (Table S2.2). Map205 is a microtubule-associated protein required for targeting Polo kinase to spindle microtubules [2]. Thus, it is likely that the effect of the Map205 knockdowns on acentric sister separation is through disruption of Polo localization. Previous studies demonstrated that Polo localizes to the DNA tether associated with the acentric and Polo knockdowns disrupted acentric transmission with sister acentrics remaining on the metaphase plate [85]. As with EB1, reductions in Map205 levels dramatically reduce the frequency of acentric separation by sliding suggesting a disruption in lateral interactions between the acentrics and

the microtubules. While much evidence indicates that Polo functions at the centromere during sister separation, our studies of the effects of Map205 and Polo knockdowns suggest that it is also involved in promoting chromatid/spindle interactions that are independent of the centromere. Reducing the levels of Topoisomerase II leads to a significant increase in failed separation of sister acentrics, supporting the conclusion that once cohesin is removed sister acentrics remain held together through DNA catenation. We suspect that reduced Topoisomerase II levels disrupt sister separation of the acentrics more profoundly than that of intact chromosomes because the latter primarily rely on kinetochore forces to resolve DNA catenations. Of the four mutants analyzed through live analysis, reductions in Topoisomerase levels had the greatest effect of the unzipping mode of acentric sister separation. This result is interesting given our finding that the unzipping mode of acentric separation is likely the most reliant on sister pairing and consequently are likely to be highly catenated.

Taken together, these data support a model in which multiple forces drive the separation of sister acentrics. Acentrics that separate by sliding and unzipping tend to be oriented parallel and perpendicular to the spindle, respectively. Unzipping could be initially driven by the DNA tether, which connects the acentric to its centric partner, to initially separate one end of the acentrics. Then, a combination of Topoisomerase II activity and microtubule forces could facilitate the separation of the other end of the acentrics. Because the partial knockdown of Topoisomerase II leads to a decreased frequency of acentrics unzipping, we hypothesize that the resolution of DNA catenations by Topoisomerase II underlies the unzipping mode of separation. Due to the finding that the tether does not appear to provide segregation forces on the acentrics [40], sliding is likely driven by lateral microtubule interactions and possibly motor proteins. This is further supported by the orientation of acentrics parallel to the

axis of polarity and the association of EB1 and bundling of microtubules around acentrics in early anaphase. It remains unclear if acentrics are directly interacting with microtubules or if microtubule-associated proteins are mediating the interaction with acentrics. There is not an obvious mechanism for the simultaneous dissociation of sister acentrics and is likely driven by a combination of factors (Figure 2.8). EB1 and Map205 may be required to establish microtubule interactions with the acentric, while in the absence of a kinetochore high levels of Topoisomerase are needed to resolve DNA catenations between sisters.

It should be noted that although these mutants resulted in a high frequency of failed acentric sister separation, we did not observe an equivalent increase in micronuclei. In contrast, mutants that disrupted acentric poleward transport or the final stages of incorporation into daughter nuclei resulted in an accompanying increase in micronuclei [41, 113, 114]. This indicates that the knockdowns in the genes identified in this study specifically disrupt acentric sister separation as the subsequent transmission occurs normally to allow incorporation of the acentric into the daughter nuclei. This interpretation is in accord with a model that acentrics experience different forces at different stages of their separation, transmission, and incorporation into daughter nuclei [113].

There are numerous examples of lateral interactions between spindle microtubules and intact chromosomes indicating that non-kinetochore forces influence anaphase chromosome kinetics [26, 33, 46]. However, it has been difficult to pursue the underlying mechanisms because of the dominance of kinetochore forces during anaphase. In analogy with studies of spindle formation in cells lacking centrosomes that led to the discovery of unsuspected, yet conserved, chromosome-based mechanisms of spindle assembly, examining the mitotic behavior of acentric chromosomes without a kinetochore will provide

insights into the kinetochore independent forces acting on intact chromosomes

[26, 33].
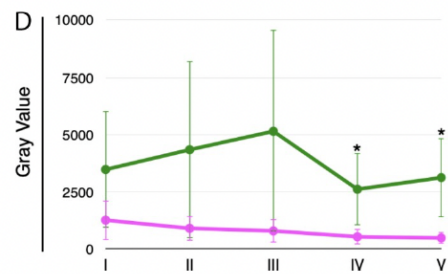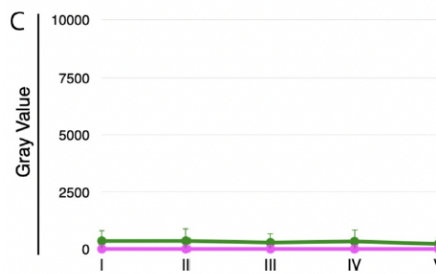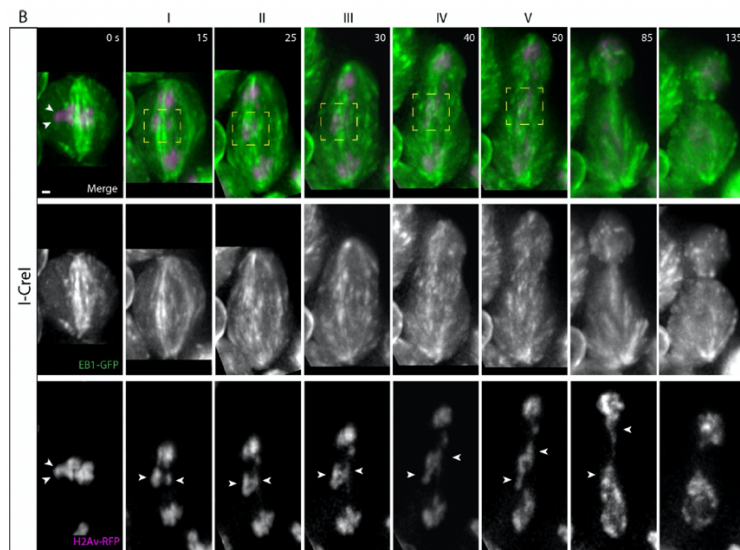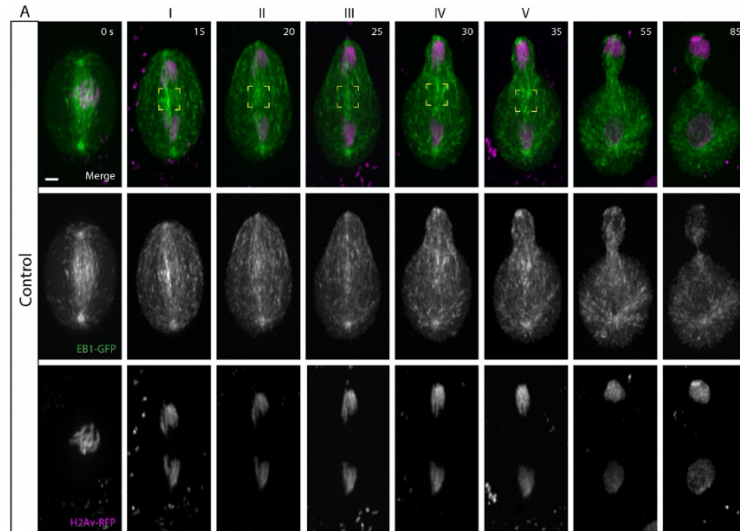
Figure 2.7: Acentrics travel poleward in late anaphase while associated with EB1. EB1 is in green and chromosomes are in magenta. (A) Still images from a time-lapse movie of a control neuroblast from metaphase (0 s) through telophase (85 s). (B) Still images from a time-lapse movie of a mitotic neuroblast with I-CreI induced acentrics from metaphase (0 s) through telophase (135 s). The intact chromosomes and acentrics initiate sister separation at the 15 s and 40 s timepoints, respectively. Sister acentrics (white arrowheads) separate and move toward opposite cell poles while associated with EB1. (C) Line graph from a compilation of five control videos showing the corrected fluorescence intensities in arbitrary units (AU) of EB1 (green) and chromosomes (magenta). Corrected fluorescence intensities were calculated within the yellow boxes at the time points 15, 20, 25, 30, 35 seconds after anaphase onset. (D) Line graph from a compilation of five videos of I-CreI-expressing neuroblasts showing the corrected fluorescence intensities in arbitrary units (AU) of EB1 (green) and chromosomes (magenta). Corrected fluorescence intensities were calculated within the yellow boxes at the time points 15, 25, 30, 40, 50 seconds after anaphase. Bars, 2 μm. Time in seconds. Error bars represent SDs of the fluorescent intensities at all points tested.
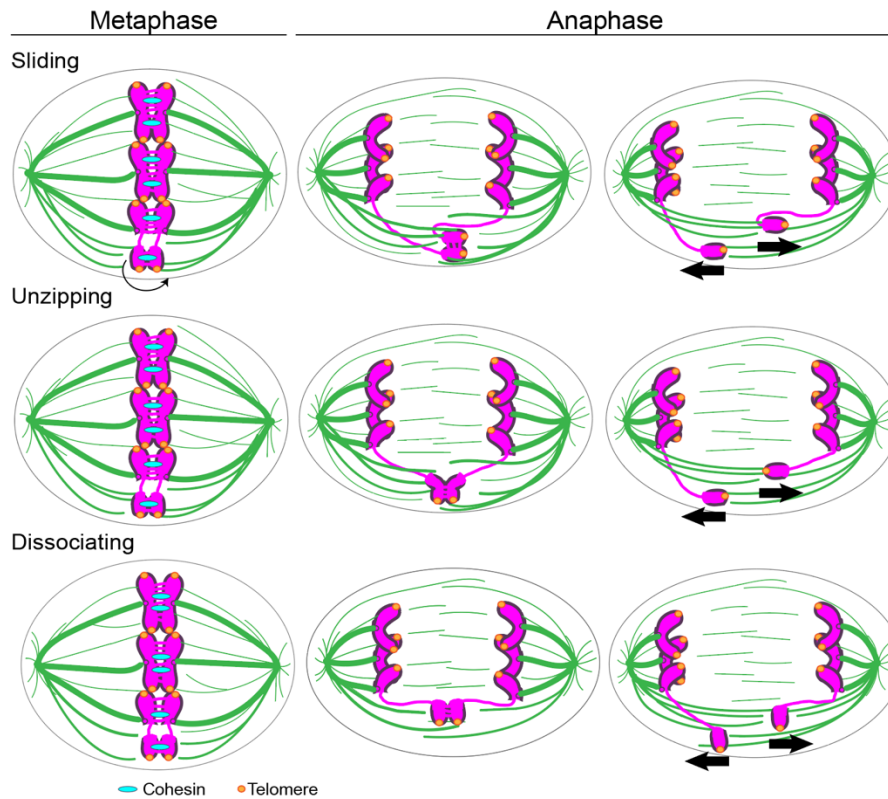
Figure 2.8: Schematic showing distinct modes of acentric separation. At some point during the metaphase- to-anaphase transition, acentrics that separate by sliding orient parallel to the spindle and slide past one another. This is likely driven by lateral associations between the microtubules and acentrics. The unzipping mode occurs when separation initiates at the broken end followed by separation of sister telomeres. It may be that the initial separation is driven by the DNA tether connecting the centric and acentric fragments. Separation across the entire length of the acentric is referred to as simultaneous dissociation. It may be that the DNA tether and acentric-microtubule interactions contribute equally for sister acentrics that separate by simultaneous dissociation. (Chromosomes in magenta, microtubules in green, cohesin in cyan, telomeres in orange).

Supplemental Figures

<div align="center">Supplemental Table: Synthetic Lethality Screen</div>

Gene (RNAi)	Stock #	I-CreI	Number of experiments	Number of Larvae per experiment	Heat Shock (1.5 hours)	Normal Adults per experiment	Mutant Phenotype per experiment	% Survival (Avg ± St Dev)	Mutant Wing Phenotype (%)
WT (control)	.	Yes	9	28,41,32,10,25,25,7,13,13	Yes	24,41,11,9,21,15, 7,9,12		80 ± 21	0
WT (control)	.	No	9	13,14,33,20,26,25,8,29,26	No	13,13,26,17,25,24,7,26,25		91 ± 7	0
Acf1	35575	Yes	1	25	Yes	17	1 with wing spot	68	4
Acf1	35575	No	1	13	No	9		69.23	0
Ada2b	35334	Yes	1	25	Yes	18		72	0
Ada2b	35334	No	1	17	No	16		94.12	0
ald	35283	Yes	1	25	Yes	13		52	0
ald	35283	No	1	25	No	22		88	0
ald	36658	Yes	1	21	Yes	14		66.67	0
ald	36658	No	1	12	No	9		75	0
Ald	26301	Yes	1	25	Yes	0	Lethal after 3rd Instar	.	.
Ald	26301	No	1	25	No	0	Lethal after 3rd Instar	.	.
asf1	35273	Yes	1	25	Yes	20	2 wing notch	80	8
asf1	35273	No	1	25	No	20	1 deformed wing	80	4
asp	28741	Yes	1	25	Yes	13		52	0
asp	28741	No	1	15	No	15		100	0
asp	35224	Yes	1	25	Yes	11	5 Wing Notch	44	20
asp	35224	No	1	25	No	24	1 Deformed wing	96	4
barr	34068	Yes	1	25	Yes	0	Lethal after 3rd Instar	.	.
barr	34068	No	1	25	No	0	Lethal after 3rd Instar	.	.
brm	34520	Yes	1	16	Yes	12		75	0
brm	34520	No	1	21	No	21		100	0
brat	34646	.	1	0	.		Lethal before 3rd instar	.	.
brat	34646	.	1	0	.		Lethal before 3rd instar	.	.
Bub1	35260	Yes	1	25	Yes	22		88	0
Bub1	35260	No	1	20	No	19		95	0
BubR1	35329	Yes	6	25,24,36,33,25,25	Yes	1,0,1,0,0,0	1 wrinkled wing	1 ± 2	4
BubR1	35329	No	3	25,16,28	No	14,4,3		31 ± 23	0
Bub3	32989	Yes	1	25	Yes	0	Adults dead inside pupae case	.	.
Bub3	32989	No	1	25	No	0	Adults dead inside pupae case	.	.
Caf1	34069	Yes	1	26	Yes	0	Lethal after 3rd Instar	.	.
Caf1	34069	No	1	23	No	0	Lethal after 3rd Instar	.	.
caf1-180	32478	Yes	1	39	Yes	0	Lethal after 3rd Instar	.	.
caf1-180	32478	No	1	25	No	0	Lethal after 3rd Instar	.	.
Cap	33431	Yes	1	25	Yes	0	Lethal after 3rd Instar	.	.
Cap	33431	No	1	13	No	0	Lethal after 3rd Instar	.	.
CAP-D2	31478	Yes	1	25	Yes	0	Lethal after 3rd Instar	.	.
CAP-D2	31478	No	1	32	No	0	Lethal after 3rd Instar	.	.
CAP-D2	31326	Yes	1	17	Yes	1		5.88	0
CAP-D2	31326	No	1	12	No	6		50	0
car	34007	Yes	1	25	Yes	19		76	0
car	34007	No	1	23	No	21		91.3	0
Cdc2	36117	Yes	1	28		0	Lethal after 3rd Instar	.	.
Cdc2	36117	No	1	18		0	Lethal after 3rd Instar	.	.
Cenp-C	34692	Yes	1	25	Yes	0	Lethal after 3rd Instar	.	.
Cenp-C	34692	No	1	22	No	0	Lethal after 3rd Instar	.	.
Cenp-C	34699	Yes	1	25	Yes	0	Lethal after 3rd Instar	.	.
Cenp-C	34699	No	1	25	No	0	Lethal after 3rd Instar	.	.
Cenp-C	26311	Yes	1	0	Yes	0	Lethal before 3rd Instar	.	.
Cenp-C	26311	No	1	0	No	0	Lethal before 3rd Instar	.	.
Chb	34669	Yes	1	27	Yes	0	Lethal after 3rd Instar	.	.
Chb	34669	No	1	22	Yes	0	Lethal after 3rd Instar	.	.
Chd1	34665	Yes	3	20,24,25	Yes	0,7,0		10 ± 17	0
Chd1	34665	No	5	20,23,13,24,19	Yes	6,9,5,7,5		33 ± 6	7
chd1	35240	Yes	1	25	Yes	12	1 with wing notch	48	4
chd1	35240	No	1	23	No	22		95.65	0
Chrac-14	35652	Yes	1	25	Yes	15	2 with wing spots	60	8
Chrac-14	35652	No	1	16	No	16		100	0
Chrac-14	31052	Yes		25	Yes	12		48	0
Chrac-14	31052	No		25	No	25		100	0
Cmet	35816	Yes	1	18	Yes	0	Lethal after 3rd Instar	.	.
Cmet	35816	No	1	25	No	0	Lethal after 3rd Instar	.	.
Cp190	33903	Yes	1	17	Yes	2		11.8	0
Cp190	33903	No	1	12	Yes	3	most dead in bottom food or "push-pop" phenotype	25	0
CtBP	32889	Yes	1	25	Yes	0	Lethal after 3rd Instar	.	.
CtBP	32889	No	1	24	No	0	Lethal after 3rd Instar	.	.
D1	33655	Yes	1	0	Yes	0	Lethal before 3rd Instar	.	.
D1	33655	No		0	No	0	Lethal before 3rd Instar	.	.
Dhc	36698	Yes	1	0	.	.	Lethal before 3rd instar	.	.
Dhc	36698	No	1	0	.	.	Lethal before 3rd instar	.	.
Dhc	28749	Yes	1	0	.	.	Lethal before 3rd instar	.	.
Dhc	28749	No	1	0	.	.	Lethal before 3rd instar	.	.
dlg	33620	.	1	0	.		Lethal before 3rd instar	.	.
dlg	33620	.	1	0	.		Lethal before 3rd instar	.	.
dpn	26320	Yes	1	25	Yes	17		68	0
dpn	26320	No	1	24	No	22		91.67	0
EB1	28605	Yes	7	10,8,7,16,6,14,25	Yes	8,6,1,4,2,5,12	11 with wing notches 1 deformed wing	44 ± 25	21 ± 6
EB1	28605	No	4	19,4,5,10	Yes	18,4,5,8		94 ± 9	0
E(bx)	33658	Yes	1	0	.	.	Lethal before 3rd instar	.	.
E(bx)	33658	No	1	0	.	.	Lethal before 3rd instar	.	.
Futch	40839	Yes	1	9	Yes	8	1 wing notch	88.9	11
Futch	40839	No	1	7	Yes	7		100	0

Gene (RNAi)	Stock #	I-CreI	Number of experiments	Number of Larvae per experiment	Heat Shock (1.5 hours)	Normal Adults per experiment	Mutant Phenotype per experiment	% Survival (Avg ± St Dev)	Mutant Wing Phenotype (%)
grp	27277	Yes	1	25	Yes	20	1-Notched wing, 1-Wing Spot, 2-Blistered wing	80	16
grp	27277	No	1	15	No	15		100	0
grp	36685	Yes	1	0	Yes	0	Lethal before 3rd instar	.	.
grp	36685	No	1	0	Yes	0	Lethal before 3rd instar	.	.
Grip75	31215	Yes	1	23	Yes	20	1 male notch	87	4
Grip75	31215	No	1	7	Yes	7		100	0
Grip84	33458	Yes	1	21	Yes	21		100	0
Grip84	33458	No	1	15	Yes	14		93.3	0
gwl	35212	Yes	1	25	Yes	22	1 Major wing spot	88	4
gwl	35212	No	1	18	No	17		94.44	0
gwl	34525	Yes	5	23,16,14,39,20	Yes	0,0,0,1,1		2 ± 2	0
gwl	34525	No	5	21,22,22,21,13	Yes	9,5,4,5,3	44 wing notches	26 ± 10	44 ± 19
hairy	34326	Yes	1	25	Yes	19		76	0
hairy	34326	No	1	25	No	25		100	0
Hira	35346	Yes	1	25	Yes	18		72	.
Hira	35346	No	1	26	No	26		100	.
His2Av	34844	Yes	1	0	Yes	0	Lethal prior to 3rd Instar	.	0
His2Av	34844	No	1	0	No	0	Lethal prior to 3rd Instar	.	0
His3.3B	34940	Yes	1	26	Yes	24	1 with blistered wing	92.31	4
His3.3B	34940	No	1	25	No	21		84	0
HmgZ	26219	Yes	1	22	Yes	17	2 notched wing	77.27	9
HmgZ	26219	No	1	25	No	16		64	0
HmgD	31344	Yes	1	25	Yes	25		100	0
HmgD	31344	No	1	25	No	23		92	0
HP1b	32401	Yes	1	20	Yes	13		65	0
HP1b	32401	No	1	25	No	21		84	0
HP1C	33962	Yes	1	25	Yes	15	2 with wing Notch	60	8
HP1C	33962	No	1	25	No	22		88	0
HP1e	34863	Yes	1	20	Yes	13		65	0
HP1e	34863	No	1	25	No	25		100	0
hyx	31722	.		25	.	0	Lethal prior 3rd instar	.	.
hyx	31722	.		25		0	Lethal prior 3rd instar	.	.
hyx	35238	Yes	1	25	Yes	2	1 deformed wing	8	4
hyx	35238	No	1	25	No	22	1 deformed wing	88	4
ial	28691	Yes	1	25	Yes	0	Lethal after 3rd Instar	.	.
ial	28691	No	1	13	No	0	Lethal after 3rd Instar	.	.
Incenp	35366	Yes	1	20	Yes	0	Lethal after 3rd Instar	.	.
Incenp	35366	No	1	17	No	0	Lethal after 3rd Instar	.	.
Ino80	37473	Yes	1	15	Yes	14		93.33	0
Ino80	37473	No	1	10	No	10		100	0
Ino80	33708	Yes	1	26	Yes	26		100	0
Ino80	33708	No	1	14	No	14		100	0
Iswi	32845	Yes	1	25	Yes	1	1 wing spot	4	4
Iswi	32845	No	1	6	Yes	0		0	0
Iswi	31111	Yes	1	40,27,36,25,25,25	Yes	17,8,26,4,11,14	1 wing notch, 3 wing spot	43 ± 20	16
Iswi	31111	No	3	42,7,40	Yes	20,6,29		69 ± 19	0
Klp68D	29410	Yes	1	24	Yes	7		29.17	0
Klp68D	29410	No	1	21	No	12		57.14	0
Klp67A	35606	Yes	1	19	Yes	10		52.63	0
Klp67A	35606	No	1	17	No	11		64.71	0
Kif3c	40886	Yes	2	18,6	Yes	10,2		44 ± 16	0
Kif3c	40886	No	1	7	Yes	2		28.6	0
Klp3A	40944	Yes	1	27	Yes	16	5 cyo adults	59.3	0
Klp3A	40944	No	1	14	Yes	9	3 cyo adults	64.3	0
klp59C	35596	Yes	1	25	Yes	23		92	0
klp59C	35596	No	1	16	No	13		81.25	0
Ku80	27710	Yes	1	25	Yes	7		28	0
Ku80	27710	No	1	25	No	24		96	0
Lok	35152	Yes	1	26	Yes	20	1 with wing spot	76.92	4
Lok	35152	No	1	25	No	24	1 with wing spot	96	4
Map60	32458	Yes	1	11	Yes	10		91	0
Map60	32458	No	1	8	Yes	8		100	0
Map205	32939	Yes	6	27,27,19,19,25,24	Yes	21,10,6,13,14,13	5 wing notches	54 ± 18	26
Map205	32939	No	6	8,15,16,10,21,21	Yes	5,12,14,8,21,19		83 ± 13	0
MCPH1	38244	Yes	1	26	Yes	9		34.6	0
MCPH1	38244	No	1	15	No	5		33.3	0
mei-41	35371	Yes	1	27	Yes	0	Lethal after 3rd Instar	.	.
mei-41	35371	No	1	25	No	0	Lethal after 3rd Instar	.	.
Mi-2	35398	Yes	1	25	Yes	0	Lethal after 3rd Instar	.	.
Mi-2	35398	No	1	24	No	0	Lethal after 3rd Instar	.	.
Mi-2	33419	Yes	2	0	Yes	0	Lethal before 3rd Instar	.	.
Mi-2	33419	No	2	0	No	0	Lethal before 3rd Instar	.	.
Mis12	38535	Yes	1	40	Yes	0	Lethal after 3rd instar	.	.
Mis12	38535	No	1	20	Yes	0	Lethal after 3rd instar	.	.
Mis12	35471	Yes	1	12	Yes	0		0	0
Mis12	35471	No	1	9	Yes	1		11.1	0
Mit(1)15	42643	Yes	1	13	Yes	11	1 blistered, 1 wing spot	84.6	15
Mit(1)15	42643	No	1	13	Yes	11		84.6	0
mor	34919	Yes	1	Dead	.		Lethal before 3rd instar	.	.
mor	34919	No	1	Dead	.		Lethal before 3rd instar	.	.
mre11	39028	Yes	1	25	Yes	0		0	0
mre11	39028	No	1	25	No	10		40	0
msps	31138	Yes	3	19,12,25	Yes	3,4,1	1 wing notch	18 ± 17	5
msps	31138	No	2	24,6	No	20,3		67 ± 24	0
mus209	33043	Yes	1	25	Yes	0	Lethal after 3rd Instar	.	.
mus209	33043	No	1	10	No	0	Lethal after 3rd Instar	.	.
mus309	31330	Yes	2	25,17	Yes	9,11		10 ± 1	0
mus309	31330	No	1	22	No	21		95.45	0

Gene (RNAi)	Stock #	I-CreI	Number of experiments	Number of Larvae per experiment	Heat Shock (1.5 hours)	Normal Adults per experiment	Mutant Phenotype per experiment	% Survival (Avg ± St Dev)	Mutant Wing Phenotype (%)
mus312	34873	Yes	1	25	Yes	0		0	0
mus312	34873	No	1	25	No	25		100	0
Nap1	35445	Yes	1	25	Yes	20	1 with wing spot	80	4
Nap1	35445	No	1	24	No	14		58.33	0
neb	28897	Yes	1	20	Yes	13		65	0
neb	28897	No	1	10	Yes	9		90	0
Nlp1	33688	Yes	2	29,25	Yes	1,0		2 ± 2	0
Nlp1	33688	No	1	6	Yes	0		0	0
NudE	38959	Yes	1	17	Yes	0	Lethal after 3rd Instar	.	.
NudE	38959	No	1	12	Yes	0	Lethal after 3rd Instar	.	.
Nuf2	35599	Yes	1	13	Yes	7		53.8	0
Nuf2	35599	No	1	8	Yes	7		87.5	0
Nuf2	36725	Yes	1	28	Yes	0	Lethal after 3rd Instar	.	.
Nuf2	36725	No	1	25	Yes	0	Lethal after 3rd Instar	.	.
Nurf-38	31341	.		0	.	0	Lethal before 3rd instar	.	.
Nurf-38	31341	.		0	.	0	Lethal before 3rd instar	.	.
Nurf-38	35444	Yes		20	Yes	0		0	0
Nurf-38	35444	No		21	No	2		9.52	0
okr	31047	Yes	1	25	Yes	12	4 with wing notches	48	16
okr	31047	No	1	15	No	10	5 with wing notches	66.67	33
par-1	32410	Yes	1	0	Yes	0	Lethal before 3rd Instar	.	.
par-1	32410	No	1	0	No	0	Lethal before 3rd Instar	.	.
par-6	35000	Yes	1	25	Yes	6		24	0
par-6	35000	No	1	15	No	3		20	0
pds5	35632	Yes	1	19	Yes	12		63.16	0
pds5	35632	No	1	20	No	16		80	0
Pbl	36841	Yes	1	16	Yes	0	Lethal after 3rd instar	.	.
Pbl	36841	No	1	16	Yes	0	Lethal after 3rd instar	.	.
Pbl	28343	Yes	2	13,28	Yes	0,0	Lethal after 3rd instar	.	.
Pbl	28343	No	2	19,23	Yes	0,0	Lethal after 3rd instar	.	.
polo	33042	Yes	1	12	Yes	0	Lethal after 3rd Instar	.	.
polo	33042	No	1	11	No	0	Lethal after 3rd Instar	.	.
Pp4-19C	27726	Yes	1	19	Yes	0	Lethal after 3rd instar	.	.
Pp4-19C	27726	No	1	26	No	0	Lethal after 3rd instar	.	.
Pp4-19C	38372	Yes	1	25	Yes	0	Lethal after 3rd instar	.	.
Pp4-19C	38372	No	1	20	No	0	Lethal after 3rd instar	.	.
PP113C	32465	Yes	1	16	Yes	0	Lethal after 3rd instar	.	.
PP113C	32465	No	1	12	No	0	Lethal after 3rd instar	.	.
PP1-87B	32414	.	1	0	.		Lethal prior to third instar	.	.
PP1-87B	32414	.	1	0	.		Lethal prior to third instar	.	.
Rpd3	34846	Yes	1	25	Yes	0	Lethal after 3rd instar	.	.
Rpd3	34846	No	1	25	No	0	Lethal after 3rd instar	.	.
Rpd3	31616	Yes	1	25	Yes	0	Lethal after 3rd instar	.	.
Rpd3	31616	No	1	25	No	0	Lethal after 3rd instar	.	.
Rtf1	31718	Yes	1	25	Yes	0	Lethal after 3rd Instar	.	.
Rtf1	31718	No	1	12	No	0	Lethal after 3rd Instar	.	.
scrib	35748	.	1	0	.		Lethal before 3rd instar	.	.
scrib	35748	.	1	0	.		Lethal before 3rd instar	.	.
Sin3A	32368	Yes	1	25	Yes	2		8	0
Sin3A	32368	No	1	25	No	6		24	0
Sir2	32481	Yes	1	25	Yes	16	3 Wing Notch, 1 Wing Spot	64	16
Sir2	32481	No	1	16	No	15		93.75	0
Sir2	31636	Yes	1	25	Yes	15	1 Wing Notch	60	4
Sir2	31636	No	1	29	No	29		100	0
SkpA	28979	Yes	1	5	Yes	0	Lethal after 3rd Instar	.	.
SkpA	28979	No	1	4	Yes	0	Lethal after 3rd Instar	.	.
SkpA	32870	Yes	1	0	.		Lethal before 3rd instar	.	.
SkpA	32870	No	1	0	.		Lethal before 3rd instar	.	.
SMC1	34351	Yes	1	25	Yes	24		96	0
SMC1	34351	No	1	11	No	11		100	0
SMC2	32369	.		0	.	0	Lethal before 3rd instar	.	.
SMC2	32369	.		0	.	0	Lethal before 3rd instar	.	.
SNF1A	32371	Yes	1	25	Yes	24		96	0
SNF1A	32371	No	1	20	No	20		100	0
Spc105R	35466	Yes	1	22	Yes	0	All dead in pupae case	.	.
Spc105R	35466	No	1	22	Yes	0	All dead in pupae case	.	.
Spd-2	36624	Yes	1	25	Yes	0	Lethal before 3rd instar	.	.
Spd-2	36624	No	1	25	No	0	Lethal before 3rd instar	.	.
Spn-A	31199	Yes	4	11,14,7,25	Yes	0,1,0,0		2 ± 4	0
Spn-A	31199	No	5	22,21,17,7,32	Yes	18,21,10,5,32		82 ± 18	0
spt4	31194	Yes	1	25	Yes	6		24	0
spt4	31194	No	1	25	No	11		44	0
spt5	34837	.		0	.		Lethal before 3rd instar	.	.
spt5	34837	.		0	.		Lethal before 3rd instar	.	.
spt6	32373	.		0	.	0	Lethal before 3rd instar	.	.
spt6	32373	.		0	.	0	Lethal before 3rd instar	.	.
sub	28570	Yes	1	25	Yes	24		96	0
sub	28570	No	1	19	No	19		100	0
Su(var)3-9	31619	Yes	1	0	Yes	0	Lethal before 3rd instar	.	.
Su(var)3-9	31619	No	1	0	No	0	Lethal before 3rd instar	.	.
Su(var)3-9	32914	Yes	1	0	Yes	0	Lethal before 3rd instar	.	.

Gene (RNAi)	Stock #	I-CreI	Number of experiments	Number of Larvae per experiment	Heat Shock (1.5 hours)	Normal Adults per experiment	Mutant Phenotype per experiment	% Survival (Avg ± St Dev)	Mutant Wing Phenotype (%)
Su(var)3-9	32914	No	1	0	No	0	Lethal before 3rd instar	.	.
Su(var)3-9	33401	Yes	1	0	Yes		Lethal before 3rd instar	.	.
Su(var)3-9	33401	No	1	0	No		Lethal before 3rd instar	.	.
Tip60	28563	Yes	1	31	Yes	0	Lethal after 3rd Instar	.	.
Tip60	28563	No	1	25	No	0	Lethal after 3rd Instar	.	.
tefu	31635	Yes	1	30	Yes	13	1 Wing Spot, 1 Wing Notch	43.33	7
tefu	31635	No	1	25	No	25		100	0
Top2	35416	Yes	1	25	Yes	0	Lethal after 3rd Instar	.	0
Top2	35416	No	1	25	No	0	Lethal after 3rd Instar	.	0
Top2	31342	Yes	1	19	Yes	0	Lethal after 3rd Instar	.	.
Top2	31342	No	1	12	Yes	0	Lethal after 3rd Instar	.	.
tou	31637	Yes	1	25	Yes	17		68	0
tou	31637	No	1	24	No	22		91.67	0
tou	35790	Yes	1	25	Yes	18	1 Wing Spot, 1 Wing Notch	72	8
tou	35790	No	1	22	No	21		95.45	0
tws	28714	Yes	2	4,14	Yes	0,0	Lethal after 3rd Instar	.	.
tws	28714	No	2	8,17	Yes	0,0	Lethal after 3rd Instar	.	.
tws	36689	Yes	1	17	Yes	16		94.1	0
tws	36689	No	1	7	Yes	7		100	0
vtd (rad21)	36786	Yes	1	25	Yes		Lethal after 3rd Instar	.	.
vtd (rad21)	36786	No	1	20	No		Lethal after 3rd Instar	.	.
woc	27057	Yes	1	25	Yes	0		0	0
woc	27057	No	1	30	No	1		3.33	0
Xnp	29444	Yes	1	25	Yes	0	Lethal after 3rd instar	.	.
Xnp	29444	No	1	11	No	0	Lethal after 3rd instar	.	.
Xnp	32894	Yes	1	11	Yes	10		90.91	0
Xnp	32894	No	1	22	No	16		72.73	0

Table S2.1: Synthetic lethality screen. 117 RNAi gene knockdowns were screened for synthetic lethal interaction upon induction of acentric chromosome formation. Percent survival was determined by taking the average number of larvae that eclosed into viable adult flies per experiment.

Mode of separation	I-CreI Alone	I-CreI, nod⁴
Sliding	48%	42%
Unzipping	22%	25%
Dissociating	13%	16%
Fails to separate	17%	17%
	N = 19	N = 12

Table S2.2: *nod* loss-of-function mutant does not disrupt the accuracy of acentric sister separation. Nod does not influence the frequencies of the three modes of acentric separation. Modes by which acentric sister chromatids separate in control cells or in *nod* mutant background. Acentric sister chromatids fail to separate, separate by sliding laterally past one another, or by unzipping from one another. Data for this table is found in [40]. All values are not statistically significant (P>0.05, two-sided t-test).

Materials and Methods

Fly stocks

All stocks were raised on standard *Drosophila* media at room temperature (20–22˚C) as previously described [85]. For generating acentrics, a transgenic fly line bearing the I-CreI endonuclease under heat-shock 70 promoter were kindly provided by Kent Golic at The University of Utah. For synthetic lethality screen, the ubiquitous Gal4 driver under the control of an actin enhancer (Act5) was used (#25708 from Bloomington). Dominant negative allele of ISWI was kindly provided by John Tamkun at UC Santa Cruz. Greatwall hypomorphs (gwl1080,716, 180, and 2790) were kindly provided by Michael Goldberg at Cornell University. The line with rad21-EGFP transgene were kindly provided by Stefan Heidmann at University of Bayreuth.

Synthetic lethality screen

Third instar progeny with genotype Act5-Gal4/+; I-CreI, Sb/UAS-RNAi were collected from parental genotypes Act5-Gal4/CyO-GFP; I-CreI, Sb/TM6B and were heat shocked for 1.5 hours at 37˚C (unless otherwise indicated). After heat shock, the vials were set-aside at room temperature for 10–15 days until adult flies emerged. Synthetic lethality was calculated as the % of larvae that develop into adulthood [40, 85]. Control progeny with genotype Act5-Gal4/+; Sb/UAS-RNAi from parents with the genotype Act5-Gal4/CyO-GFP; Sb/TM6B and UAS-RNAi were heat-shocked for 1.5 hours at 37˚C.

Live analysis of acentric behavior in *Drosophila* third instar neuroblasts

As previously described, acentric chromosome fragments were induced by I-CreI expression (under heat shock 70 promoter) in 3rd instar larvae by a 1-

hour 37˚C heat shock followed by a 1-hour recovery period at room temperature [40]. The larval brains from third instar larvae were dissected in PBS and then transferred to a slide with 20 µl of PBS. A coverslip was dropped on PBS with brain and the excess PBS was wicked out from edge of coverslip to induce squashing of brain between slide and coverslip. For live analysis, the edge of coverslip was sealed with halocarbon and was imaged as described below. Neuroblast divisions in all images were from female 3rd instar larvae.

Microscopy and image acquisition

      Wide-field microscopy. Time-lapse imaging for Figs 4C, 4D, 5C and 6 were performed using a Leica DM16000B wide-field inverted microscope equipped with a Hamamatsu electron-multiplying charge coupled device camera (ORCA 9100–02) with a binning of 1 and a 100x Plan-Apochromat objective with NA 1.4. Successive time points were filmed at 20 s. RFP (585 nm) and GFP (508 nm) fluorophores were imaged. Samples were imaged in PBS and at room temperature (20–22˚C). Widefield images were acquired with Leica Application Suite Advanced Fluorescence Software and 3D deconvolved using AutoQuant X2.2.0 software.

      Spinning-disk microscopy. Images in Figs 1, 2, 3, 4, 6, and 7 were acquired with an inverted Nikon Eclipse TE2000-E spinning disk (CSLI-X1) confocal microscope equipped with a Hamamatsu electron-multiplying charge coupled device camera (ImageEM X2) with a 100X 1.4 NA oil-immersion objective. Samples were imaged in PBS and at room temperature (20–22˚C). Images were acquired with MicroManager 1.4 software. Time-lapse fluorescent images of neuroblasts divisions were done with 120 and 100 ms exposures for GFP and RFP respectively with 0.5 µm Z-steps. Time-lapse videos with both GFP and RFP were done every 5 to 9 seconds and time-lapse movies with RFP

alone were done every 5 seconds. Figures were assembled in Adobe Illustrator.

Selected stills (both experimental and control) were processed with ImageJ

(http://rsb.info.nih.gov/ij/)).

Measurements

In Fig 2C, relative fluorescence intensities of chromosomes (H2Av-RFP)

and cohesin (Rad21 EGFP) were done using the plot profile function in ImageJ of

the region outlined around acentrics and the main mass of chromosomes. In Fig

7C and 7D, relative fluorescence intensities of acentrics (H2Av-RFP) and EB1

(EB1-EGFP) were done using the plot profile function in ImageJ of the region

outlined around acentrics in I-CreI expressing neuroblasts and the region

outlined around the spindle midzone in control neuroblasts. For statistical

analyses, unpaired two-sided t-tests and two-sided Mann-Whitney-Wilcoxon tests

were used. Unpaired two-sided t-tests were performed in Prism Version 8

(GraphPad Software). Two-sided Mann- Whitney-Wilcoxon tests were performed

in R (R Core Team) and Prism Version 8 (GraphPad Software).

Chapter 3: Acentric chromosomes congress via kinetochore-independent forces and induce a global reorganization of chromosomes at the metaphase plate

Abstract

Chromosome congression, the alignment of chromosomes on the metaphase plate in preparation for sister separation at anaphase, relies heavily on a combination of microtubule plus-end and lateral interactions with the kinetochore. Currently unclear are the kinetochore-independent forces that drive congression. Here we take advantage of our ability to efficiently generate a GFP-marked acentric X chromosome fragment in *Drosophila* neuroblasts to identify forces acting on chromosome arms that drive congression. We find acentrics efficiently congress to the metaphase plate, often more rapidly than kinetochore-bearing chromosomes. However, the congressed acentrics are positioned in a plane distinct, and significantly further, from the chromosome-free center of the ring of intact chromosomes. Examination of monopolar spindles reveals the acentric experiences robust plus-end directed forces. We also find that acentric congression relies on a combination of EB1 mediated plus-end microtubule pushing forces and migration along microtubules via the KLP3A chromokinesin. Taken together these studies demonstrate that congression involves microtubule lateral and plus-end interactions with the kinetochore and the chromosome arms. Our studies also reveal that the congressed chromosomes in *Drosophila* neuroblasts are arranged in an irregular column perpendicular to the spindle axis. However, upon induction of acentric chromosome fragments, the intact chromosomes organize into a distinct torus shape on the metaphase plate. This reorganization of congressed chromosomes depends on the activation of the

DNA damage checkpoint kinases Chk1 and Chk2. Irradiation experiments reveal DNA damage, rather than the generation of an acentric chromosome fragment drives the reorganization of congressed chromosomes into a torus.

Introduction

Chromosome fragments lacking a centromere and a telomere are known as acentrics. Due to their lack of a kinetochore, acentrics are unable to make canonical attachments to microtubules. Kinetochore-microtubule interactions play key roles in mediating chromosome congression to the spindle equator, sister chromosome separation during the metaphase-to-anaphase transition and segregation during anaphase [62]. Thus, acentrics were expected to fail to align properly on the metaphase plate, display separation and segregation defects in anaphase, be excluded from daughter nuclei in telophase, and form cytoplasmic micronuclei [23, 38, 48]. Surprisingly, multiple reports have found acentric chromosome fragments often display proper sister chromosome separation and poleward migration, and inclusion into daughter nuclei [4, 9, 37, 40, 41, 44, 50, 85, 109, 113, 114]. Proposed mechanisms include neo-centromere formation and direct association of acentrics with microtubules or a kinetochore-bearing chromosome [35, 36, 40, 65, 78, 115]. Studies have shown that separation of sister acentric chromosomes during early anaphase relies on Topoisomerase II activity as well as microtubule plus-end pushing forces [109]. Additional work has shown that the anaphase poleward segregation of acentric chromosomes involves Klp3A mediated microtubule-based movement [40].

Here we explore the mechanisms that drive congression and alignment of acentric chromosome fragments at the metaphase plate as this also provides insight into the non-kinetochore forces driving congression of intact

48

chromosomes. As with sister chromosome separation and segregation, the kinetochore plays a key role in chromosome congression.   Following nuclear-envelope breakdown, chromosomes positioned within the microtubule arc bounded by the centrosomes quickly establish lateral interactions with the plus-end kinetochore-associated motor protein CENP-E and are transported to the metaphase plate [53]. This is referred to as direct congression. Once at the equator, lateral interactions are converted to plus-end microtubule interactions and the sister kinetochores establish biorientation with microtubules attached to opposing poles [98]. Opposing forces at the sister kinetochores and chromosome arms result in oscillations but maintain the chromosomes at the metaphase plate. Polar ejection forces mediated by plus-end microtubule dynamics and chromokinesins acting on the chromosomes also drive chromosomes away from the poles toward the equator [53, 98]. Congression of chromosomes located at the spindle periphery and outside of the centrosome-metaphase plate region at the time of nuclear envelope breakdown require an additional step, known as peripheral congression. They must first rely on kinetochore-associated Dynein for microtubule minus-end directed transport to the spindle pole. Once at the pole, the chromosomes engage CENP-E for transport to the metaphase plate. [53].

In spite of the key role of the kinetochore in driving congression, acentric chromosome fragments are capable of movement toward and alignment at the metaphase plate [4, 11, 40, 42, 83, 85, 109]. This was dramatically demonstrated through live analysis of acentric fragments generated via laser ablation. These fragments rapidly moved away from the poles at a rate similar to intact chromosomes [83]. Subsequent live analysis of X-chromosome acentric fragments generated through endonuclease induction in *Drosophila* neuroblasts revealed they also experience robust poleward forces and are capable of aligning on the metaphase plate [40, 85, 109, 113].

Left unresolved are the mechanisms driving congression of chromosome fragments lacking a kinetochore. Here we explore this issue by taking advantage of our ability to efficiently generate GFP-labeled acentric fragments in the genetically tractable *Drosophila* neuroblasts. The GFP tag facilitates tracking of the acentric from the pole to the metaphase plate. We find acentrics frequently arrive and align at the metaphase plate before the kinetochore-bearing chromosomes and are positioned away from the main mass of chromosomes. Examination of monopolar arrays reveals acentrics experience robust poleward forces. Functional analysis reveals acentric congression relies on a combination of EB1 mediated plus-end microtubule pushing forces and migration along microtubules via the KLP3A chromokinesin. Taken together these studies demonstrate that congression involves microtubule lateral and plus-end interactions with the kinetochore and the chromosome arms. In addition, we demonstrate that the double-strand breaks generated upon acentric induction results in a global reorganization of the congressed metaphase chromosomes. Normally, the congressed chromosomes are organized in a loosely parallel configuration on the metaphase plate. Induction of the DSBs either via I-CreI or X-ray irradiation results in the congressed chromosome forming a distinct torus configuration. This global reorganization of the metaphase chromosomes requires the cell cycle checkpoint functions of both Chk1 and Chk2.

Results

Acentric sister chromatids congress to the metaphase plate faster than kinetochore-bearing chromosomes

As previously described, acentric chromosome fragments have the remarkable ability to congress to the metaphase plate, separate and segregate

50

from one another in anaphase, and incorporate into the reforming daughter nuclei, all while lacking canonical kinetochore-microtubule attachments [109, 113]. However, because the acentric fragment has not been marked it was not always possible to track the acentric fragment throughout the entirety of mitosis. We addressed this issue by taking advantage of a GFP marker that specifically tags the *Drosophila* X chromosome. In *Drosophila*, the male-specific lethal (MSL3) complex plays a major role in dosage compensation by upregulating genes on the male X chromosome [96]. MSL3-GFP preferentially binds the male X euchromatin and thus is suitable for distinguishing the X chromosome from the other chromosomes in live studies. Acentrics were generated using heat-shock-induced expression of the I-CreI endonuclease, which targets rDNA repeats embedded in the X-chromosome centric heterochromatin producing a kinetochore-bearing heterochromatic chromosome fragment and a euchromatic acentric chromosome fragment [28]. As MSL3-GFP specifically localizes to the euchromatin, it preferentially labels the acentric chromosome fragment and is readily tracked over the course of a mitotic division (Figure 3.1). The MSL3-GFP marker does not disrupt acentric chromosome congression, segregation, or micronuclei formation when compared to control cells with acentrics alone (Figure S3.1).

These analyses reveal that, on average, acentric X chromosomes move at a significantly faster rate to the metaphase plate (11.7 ± 3.5 nm/s, N=14) when compared to intact X chromosomes (8.4 ± 3.3 nm/s, N=12, P=0.01, Mann-Whitney Test) (Table 3.1). Intact autosomes (8.5 ± 2.4 nm/s, N=28) congress to the metaphase plate at a rate in accordance with the intact X chromosomes (8.4 ± 3.3 nm/s, N=12, P=0.6, Mann-Whitney Test) (Table 3.1).
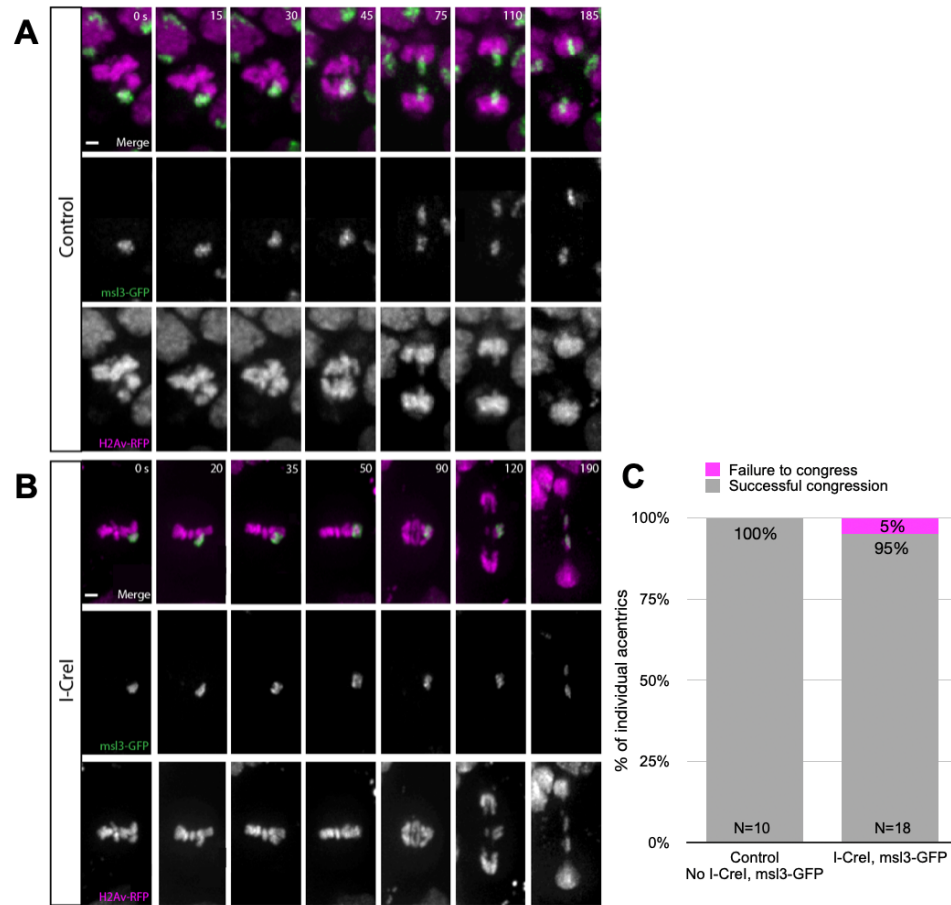
Figure 3.1: Acentrics can congress to the metaphase plate. (A) Still frames of a time-lapse movie of a mitotic neuroblast labeled with H2Av-RFP (magenta) and msl3-GFP (green) not expressing I-CreI. (B) Still frames of a time-lapse movie of a mitotic neuroblast with I-CreI induced acentrics. Sister acentrics lag on the spindle equator but eventually separate, segregate, and are incorporated into daughter nuclei. Bars, 2 μm. Time in seconds. (C) Bar graph showing the rate of chromosome congression to the metaphase plate. Successful chromosome congression is in gray. Failure of chromosomes to congress is in magenta.

	Avg velocity ± SD (nm/s)	N (individual chromosomes)
Intact X chromosomes	8.4 ± 3.3	12
Non-X chromosomes	8.5 ± 2.4	28
Acentric X chromosomes	11.7 ± 3.5	14

Table 3.1: Average velocities of chromosomes to the metaphase plate.
Depicted above are the velocities of individual acentrics as they travel to the metaphase plate. Velocity is measured in nanometers per second. Congression velocity is defined as beginning when chromosomes are distinctly visible during prometaphase and ends one frame prior to anaphase onset. Asterisks indicate statistical significance (*P=0.005, **P=0.01) as determined by a two-sided Mann-Whitney test.

I-CreI-induced DNA damage results in an Chk1/Chk2-dependent global reorganization of the congressed chromosomes on the metaphase plate

It is well established that sister chromatids align at the metaphase plate along the spindle midzone. However, the effects of DNA damage and acentric production on the global organization of the entire chromosome complement have not been explored. Here we address this issue by acquiring multiplane images of congressed chromosomes in live *Drosophila* neuroblasts in which I-CreI expression was or was not induced. In wild-type neuroblasts in which I-CreI was not induced, merging of the multiplane Z stacks reveals the chromosomes are aligned in a column configuration during metaphase (N=5, Figure 3.2).

Unexpectedly, we discovered that the alignment of the chromosomes on the metaphase plate is globally altered upon I-CreI expression. The congressed chromosomes form a torus (donut) shape aligned on the metaphase plate in a circular configuration with chromosomes absent in the center (N=5, Figure 3.2).

To test if the induction of the torus configuration of congressed chromosome is due to generation of a large acentric chromosome fragment or the I-CreI-induced DNA damage, we examined chromosome congression in neuroblasts exposed to X-ray irradiation. This analysis revealed that the chromosomes do form a torus configuration in response to radiation-induced DNA damage (Figure S3.2).

To determine if the DNA damage-induced reorganization of the congressed chromosomes into a torus requires the DNA damage checkpoint, we conducted 3D image analysis on metaphase cells expressing I-CreI and RNAi against a key kinase in the DNA Damage Response, Loki (Chk2) [55]. Analysis of metaphase cells revealed that the congressed chromosomes do not form a torus, rather they align in a crescent formation similar, but not identical, to the wild-type congressed column chromosome formation (N= 6, Figure 3.3). We also examined the role of another key kinase involved in the DNA Damage Response, Grapes (Chk1) [24, 82]. Analysis of 3D image renderings of metaphase cells expressing I-CreI and a loss-of-function *grapes* mutant revealed that the congressed chromosomes fail to form a torus and are arranged in a crescent-like formation similar to that observed in cells expressing *loki* (Chk2) RNAi (N=6, Figure 3.3).

To quantify these analyses, we measured the circularity of the entire congressed mass of chromosomes at metaphase. Perfect circles have a circularity of 1. Measurements of circularity show these crescent formations are significantly distinct from the torus shapes seen in neuroblasts only expressing I-CreI (Figure 3.3E). The average circularity of metaphase congressed chromosomes with acentrics was 0.95 (SD=0.013, N=6). The average circularity of congressed chromosomes in *grapes* mutant background decreased to 0.62 (SD=0.18, N=6). Likewise, the average circularity in *loki* RNAi-expressing cells was 0.73 (SD=0.10, N=6). Interestingly, 83% (5/6) of acentric sisters are able to congress to the metaphase plate in *grapes* mutant background (Control: I-CreI alone, 95% N=18; Figure 3.3F). Similarly, 83% (5/6) of acentric sisters align at metaphase after expression of *loki* RNAi (Figure 3.3F). Taken together these studies indicate that it is activation of the DNA Damage Response rather than the

presence of the acentric that induces the formation of a torus configuration of

congressed chromosomes.
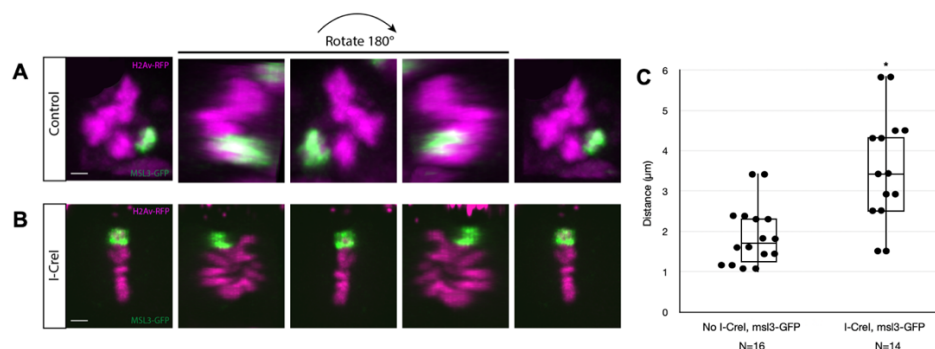
Figure 3.2: Acentrics congress to the chromosomal mass periphery. (A) Still images of a 3D rendering of a neuroblast at metaphase labeled with H2Av-RFP (magenta) and msl3-GFP (green) not expressing I-CreI. (B) Still frames of a 3D rendering of a neuroblast at metaphase with I-CreI induced acentrics. Bars, 2 µm. Images are rotated 180°. (C) Box plot showing the distances of X chromosomes from the chromosome mass center. Distances are measured µm. Acentric X-chromosomes are positioned significantly farther from the chromosome mass center when compared to the intact X-chromosome (*P=0.01, Mann-Whitney Test).
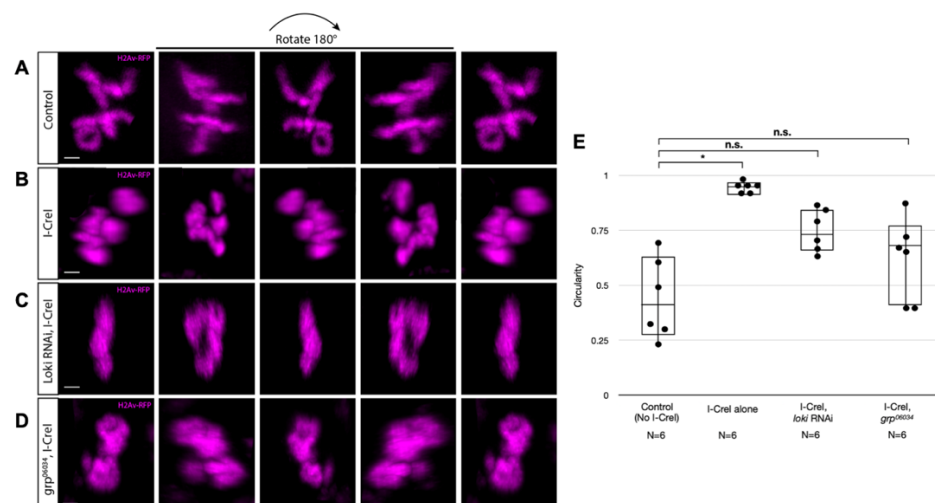
Figure 3.3: The DNA Damage Response triggers a global rearrangement of chromosomes at metaphase. (A) Still images of a 3D rendering of a neuroblast at metaphase labeled with H2Av-RFP (magenta) not expressing I-CreI. (B) Still frames of a 3D rendering of a neuroblast at metaphase with I-CreI induced acentrics. (C) Still images of a 3D rendering of a neuroblast at metaphase expressing I-CreI and *loki* RNAi. (D) Still images of a 3D rendering of a neuroblast at metaphase expressing I-CreI and a loss-of-function *grp^06034* mutant. Bars, 2 µm. Images are rotated 180°. (C) Box plots showing the circularity of the

chromosome mass at metaphase immediately prior to anaphase onset. Perfect circles have a circularity of 1. (*P=0.005, not significant at P>0.05, Mann-Whitney Test).

Acentric chromosomes are preferentially positioned at the periphery of the main mass of congressed chromosomes

Metaphase images of labeled intact X chromosomes reveal that it is aligned with the autosomes in a planar columnar configuration. In addition, the intact X chromosome is consistently positioned at the outer edge of the column of congressed chromosomes (Figure 3.2, N=5). On average, acentric X chromosomes are positioned significantly farther (3.60 ± 1.34 µm, N=14) from the chromosomal mass center when compared to intact X chromosomes (1.89 ± 0.74 µm, N=16) (Figure 3.2, P=0.01, Mann-Whitney Test). The center of the mass of intact chromosomes was determined by defining the upper, lower, left, and right boundaries of the torus and calculating the center point. As described above, acentric X chromosome fragments efficiently congress to the metaphase plate but reside in a position distinct from the main chromosome complement (Figure 3.1). 72% (10/14) of acentric X chromosomes and 38% (6/16) of intact X chromosomes reside in a Z-plane (Z-step size= 0.5 µm) separate from the Z planes in which the kinetochore-bearing congressed chromosomes reside.

## Acentrics rotate while moving to the metaphase plate

In prometaphase, sister acentrics in both male and female *Drosophila* neuroblasts travel to the metaphase plate while remaining paired together. This is likely due to the presence of cohesin protein complexes and DNA catenations between acentric sisters [109]. Similarly, kinetochore-bearing chromosomes

travel to the metaphase plate with their sister centromeres and chromosome arms paired together.

Previous work demonstrated that the orientation of acentrics at the metaphase-to-anaphase transition correlates with their mode of separation during late anaphase [109]. To investigate if the orientation of acentrics remains constant leading up to the metaphase-to-anaphase transition, we measured the orientation angles of acentric and intact X chromosomes during the 80-second interval prior to anaphase onset (Figure 3.4). Kinetochore-bearing sister chromatids align at the metaphase plate undergoing few rotations, most often remaining perpendicular to the mitotic spindle (Figure 3.4A & 3.4C). However, acentric sisters rotate several times as they line up at the metaphase plate, alternating between orienting parallel and perpendicular to the spindle and division axis (Figure 3.4B & 3.4C).

To investigate the dynamics of acentric sister congression, we imaged live neuroblasts expressing inducible I-CreI, the histone marker H2Av-RFP, and the telomere marker HOAP-GFP [12]. Marked telomeres allowed us to determine the orientation of acentrics with respect to one another as they aligned on the metaphase plate. 88% (30/34) of acentric sister pairs were oriented with telomeres paired and aligned, whereas 12% (4/34) of acentrics had telomeres oriented in opposing directions (Figure 3.5B & 3.5C). In comparison, 100% (25/25) of intact chromosomes had telomeres paired and aligned and 0% (0/25) had telomeres oriented in opposing directions (Figure 3.5A & 3.5C). These findings indicate the kinetochore plays a key role in maintaining the fidelity of sister chromosome alignment in *Drosophila*.
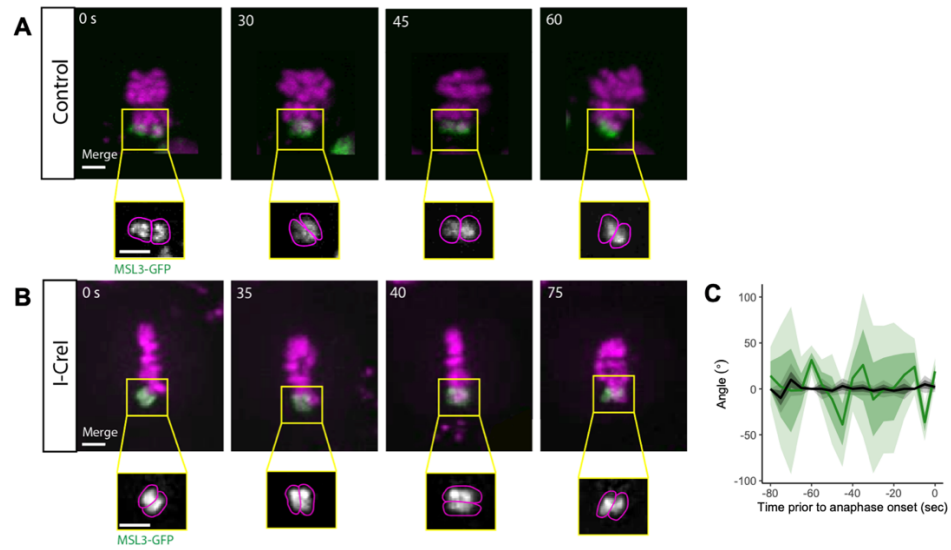
Figure 3.4: Acentrics undergo varied orientations during metaphase (A) Still frames of a time-lapse movie of a mitotic neuroblast labeled with H2Av-RFP (magenta) and msl3-GFP (green), not expressing I-CreI, during metaphase. Zoomed in images show only the X chromosomes marked by msl3-GFP (gray). (B) Still frames of a time-lapse movie of a mitotic neuroblast with I-CreI induced acentrics during metaphase. Zoomed in images show only the X chromosomes marked by msl3-GFP (gray). Bars, 2 µm. Time in seconds. (C) Line graph showing the change in orientation of acentric (green) and intact (black) X chromosomes over time, prior to anaphase onset. Shaded regions represent one- and two-times the standard deviation.
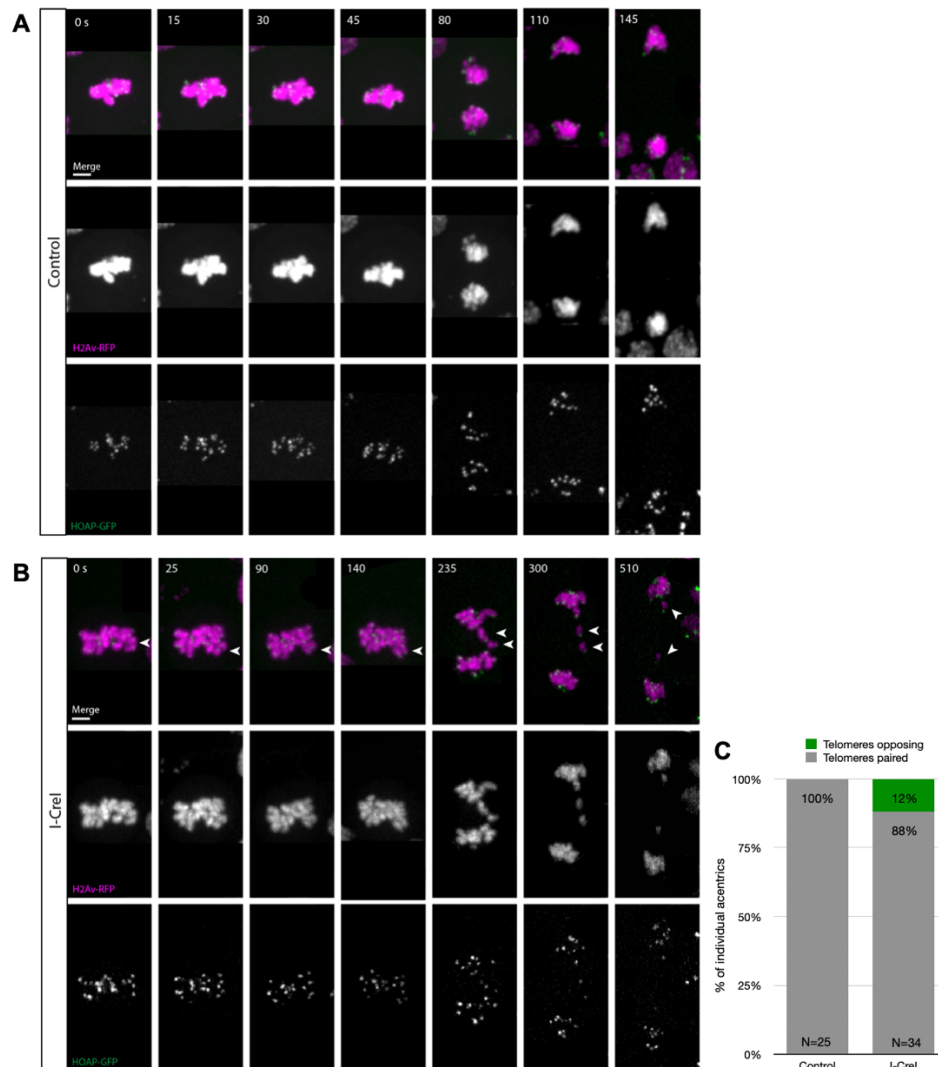
Figure 3.5: Acentrics align at the metaphase plate with telomeres paired.
(A) Still frames of a time-lapse movie of a mitotic neuroblast labeled with H2AvRFP (magenta) and HOAP-GFP (green) not expressing I-CreI. (B) Still frames of a time-lapse movie of a mitotic neuroblast with I-CreI induced acentrics (white arrowheads). Most acentrics are oriented with their telomeres paired during metaphase. Bars, 2 μm. Time in seconds. (C) Percentages of individual acentrics oriented with their telomeres paired or opposing during metaphase.

Acentric congression requires microtubule plus-ends

Previous studies in *Drosophila* reported the microtubule-stabilizing protein Map205 and the microtubule plus-end associated protein EB1 were found to be crucial for separating acentric sisters during anaphase [109]. To test if

acentrics are being acted on by microtubule plus-ends, we re-analyzed published

data of cells expressing RNAi against the microtubule plus-end tracking protein

EB1 [109]. Our re-analysis uncovered defective congression of acentric sisters to

the metaphase plate with 27% (8/30) of acentric sisters unable to align with

kinetochore-bearing chromosomes (Figure S3.3).

A separate study demonstrated that peripheral interpolar microtubules

play a critical role in the poleward segregation of acentric chromosome fragments

[40]. Disruption of interpolar microtubule organization via knockdown of Klp3A

(kinesin-4), inhibits the segregation of acentric, but not intact chromosomes.

Additional laser-ablation experiments demonstrated that segregating acentrics

are physically connected to the interpolar microtubules [40]. To determine if

microtubules and motor proteins are driving acentric congression, we live-imaged

dividing neuroblasts expressing I-CreI and RNAi against the chromokinesin

Klp31E (kinesin-4). The Klp31E ortholog in *C. elegans*, Klp-12, is involved in

chromosome congression to the metaphase plate as well as chromosome

segregation in anaphase [92]. However, in *Drosophila* S2 cells, RNAi knockdown

of Klp31E produced no mitotic phenotype [29]. Interestingly, we find in

Drosophila neuroblasts, partial knockdown of Klp31E using RNAi reveals

disruptions in interpolar microtubule organization as well as inefficient movement

of centrosomes to opposite cell poles, the latter giving an appearance of a

monopolar spindle (Figure 3.6). In these *Drosophila* neuroblasts with monopolar

spindles, the acentric chromosomes, as well as the intact chromosomes, are

pushed to the cell periphery (Figure 3.6B). This finding indicates acentric

chromosomes can be driven to microtubule plus ends prior to the metaphase-to-

anaphase transition without requiring kinetochores. It remains to be determined if

the acentrics are directly interacting with microtubule plus ends or utilizing motor

proteins to travel to the microtubule plus ends. Surprisingly, despite this cellular

defect of monopolar spindles, neuroblasts form an acentrosomal bipolar spindle allowing cells to successfully divide. 92% (14/15) of acentrics are able to line up at the metaphase plate, with 80% (12/15) of acentric sisters successfully separating and segregating from one another and moving to opposite cell poles (Figure 3.6C & 3.6D).
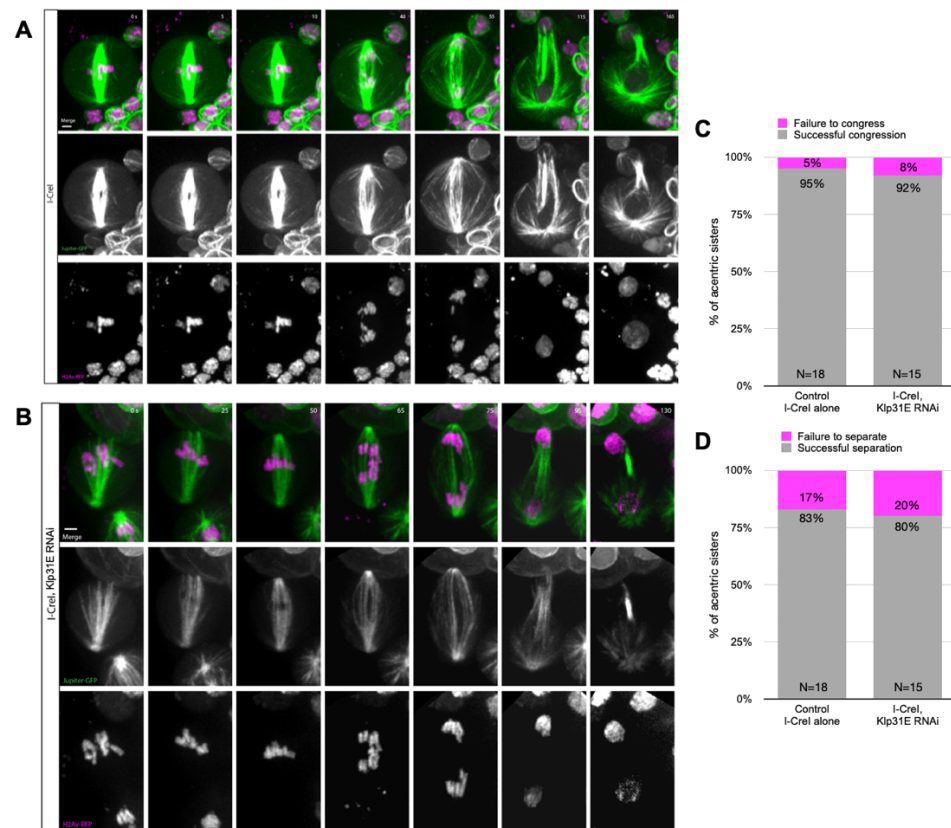
Figure 3.6: Acentrics are pushed by microtubule plus-ends (A) Still frames of a time-lapse movie of a mitotic neuroblast expressing H2AvRFP (magenta) and Jupiter-GFP (green) with I-CreI induced acentrics. Sister acentrics (white arrowheads) congress to the metaphase plate and lag behind at the spindle equator but eventually separate, segregate, and are incorporated into daughter nuclei. (B) Still frames of a time-lapse movie of a mitotic neuroblast with I-CreI induced acentrics and expressing Klp31E RNAi. All chromosomes are pushed to the cell periphery by the mono-polar mitotic spindle. Bars, 2 μm. Time in seconds. (C) Percentages of acentric sisters that fail to congress to the metaphase plate. (D) Percentages of acentric sisters that fail to separate from one another during late anaphase.

Discussion

The kinetochore plays a key role in chromosome congression. Kinetochore-associated motor proteins CENP-E and Dynein mediate lateral and plus-end microtubule interactions that propel chromosomes to the metaphase plate [53]. Congression is further facilitated by microtubule-based polar-ejection forces acting along the chromosome arms [53]. Analysis of the behavior of acentric chromosome fragments reveal forces independent of the kinetochore are sufficient to efficiently drive chromosomes to the metaphase plate. Here, taking advantage of our ability to fluorescently tag the *Drosophila* X-chromosome acentric, we define the forces acting on the chromosome arms and the role of the kinetochore in chromosome congression.

A key finding of our analysis is that acentrics congress to the plate at a rate significantly faster than kinetochore-bearing chromosomes. This indicates that kinetochore microtubule interactions actually act as a brake during congression and is in line with studies of other microtubule-based motor proteins [34, 99]. In *Drosophila* and *Xenopus*, kinesin-5 and kinesin-14 were found to generate antagonistic sliding forces aiding in the separation of spindle poles [34, 99]. Thus, with the kinetochore acting as a common rate-limiting step, this restricts the window of time in which the chromosomes reach the metaphase plate. Our analysis also demonstrates that in contrast to intact chromosomes, paired sister acentrics rotate during their migration to the metaphase plate. The most likely explanation is that in the absence of a kinetochore, polar ejection forces unevenly distributed along the length of the chromosome dominate causing rotation. This suggests that the kinetochore-microtubule interaction stabilizes chromosome orientation during congression.

We also find that the acentric is positioned at the periphery of the metaphase plate often on a plane distinct from the rest of the chromosome

complement. Previous studies demonstrated that the peripheral interpolar microtubules play a key role in acentric segregation during anaphase [40]. The positioning of the acentrics at the edge of the metaphase plate, while associating with interpolar microtubules, indicates that this microtubule population is also relied on for acentric chromosome congression. These results are in accord with the finding that knockdown of Klp3A, a plus-end directed motor protein responsible for establishing the population of interpolar microtubules, preferentially disrupts congression of acentric chromosomes [39, 40]. Previous work uncovered that *Drosophila* neuroblasts homozygous for hypomorphic alleles of *klp3A*, displayed erroneous congression of the acentrics, but not the intact chromosomes [39]. In neuroblasts expressing I-CreI, 10% (2/21) of acentrics fail to align properly at metaphase [39]. However, in *klp3A* mutant neuroblasts expressing I-CreI, 30% (6/20) of acentrics fail to align with kinetochore-bearing chromosomes at the metaphase plate [39]. It remains to be determined if Klp3A directly interacts with acentrics to aid in their transport to the metaphase plate. Acentrics could be traveling along interpolar microtubules via Klp3A, an unknown motor protein, or by directly attaching to microtubules either laterally or end-on.

Our studies also demonstrate that polar ejection forces play significant roles in acentric congression. This is most dramatically illustrated by the fact that reduction of EB1 activity preferentially disrupts congression of the acentric but not the intact chromosomes. EB1 has been found to be essential for generating anti-polar forces on chromosomes and stabilizing microtubules [101, 110]. This finding is also supported by the finding that in monopolar spindles acentrics, as well as intact chromosomes, are pushed away from the poles. Additionally, we find the acentrics frequently alternate between orienting perpendicular and

parallel to the mitotic spindle, whereas intact chromosomes largely remain perpendicular, before the metaphase-to-anaphase transition.

Thus, we suspect a combination of end-on microtubule interactions as well as lateral microtubule interactions are driving acentric chromosome congression (Figure 3.7). By labeling the telomeres of chromosomes, we determined the orientation of paired sister acentrics as they congressed and aligned on the plate. Intact sister chromatids exhibit parallel alignment across the entire length of the chromosome. This gene-for-gene alignment of paired sisters likely facilities their stable cohesion and mitotic recombination [13, 51]. Surprisingly, we found that a small but significant fraction of sister acentrics align in an anti-parallel orientation. To our knowledge this is a novel demonstration that gene-for-gene alignment is not required for sister chromatid cohesion. It also indicates that the kinetochore is required to prevent antiparallel alignment of sister chromatids, as parallel alignment of sister chromatids could facilitate proper biorientation of telocentric, acrocentric, or submetacentric chromosomes. The mechanism by which the kinetochore facilitates parallel alignment remains mysterious as it is likely established during interphase immediately following completion of S-phase [93].

A completely unexpected finding from this analysis is that the presence of the acentric chromosome fragment induces a global reorganization of chromosomes in *Drosophila* neuroblasts. In wild-type *Drosophila* cells, chromosomes align themselves in a column formation at metaphase. However, in the presence of the acentric chromosome fragment, the chromosomes arrange themselves in a torus configuration. Interestingly, this torus configuration of chromosomes at metaphase is well-documented in human cells [74]. 3D-reconstructions of human metaphase chromosomes reveal their arrangement in a circular shape with kinetochores organized around the center and chromosome

64

arms pushed towards the cell periphery [74]. Although, human cancer cell lines often contain damaged DNA which could contribute to the toroidal shape of the chromosome mass at metaphase [49, 107]. A similar torus configuration of congressed chromosomes has been observed in diatoms. In these species, interpolar microtubules gather in the center of the cell at metaphase, connecting spindle poles, and push chromosomes to either side of the interpolar microtubule bundle [76]. Additionally, in prometaphase newt pneumocytes, bundles of keratin filaments push chromosomes to the cell periphery [32]. However, in *Drosophila* neuroblasts expressing I-CreI, the mitotic spindle is arranged with microtubules connecting to congressed chromosomes in the torus formation and an absence of microtubules in the center of the torus (Figure S3.4). Whether this torus orientation is common is other cell types remains to be determined.

Whether it is the presence of the acentric or damaged DNA that causes the global reorganization of the congressed chromosome remains unclear. The DNA Damage Response serves as a canonical regulatory pathway for the cell to repair any DNA damage before the conclusion of mitosis [6]. In the event that DNA damage is present during early mitosis, the cell will arrest at metaphase to ensure the DNA damage is resolved before proceeding into anaphase [16, 54, 72]. To determine if the DNA Damage Response is triggering this restructuring of congressed chromosomes, we partially knocked down the DNA Damage Response kinases Grapes (Chk1) and Loki (Chk2) in *Drosophila* neuroblasts. We find upon disruption of Grapes (Chk1) and Loki (Chk2) function, chromosomes arrange in a crescent formation, more closely resembling wild-type configuration. To our knowledge this is the first demonstration that the DNA damage response plays a role in organizing damaged chromosomes on the metaphase plate. Whether this activity is specific to *Drosophila* remains unclear. The function of the toroidal chromosome organization also remains to be determined. One potential

explanation is the toroidal chromosome organization acts as a protective

mechanism preventing erroneous attachment of the acentric to another

chromosome.
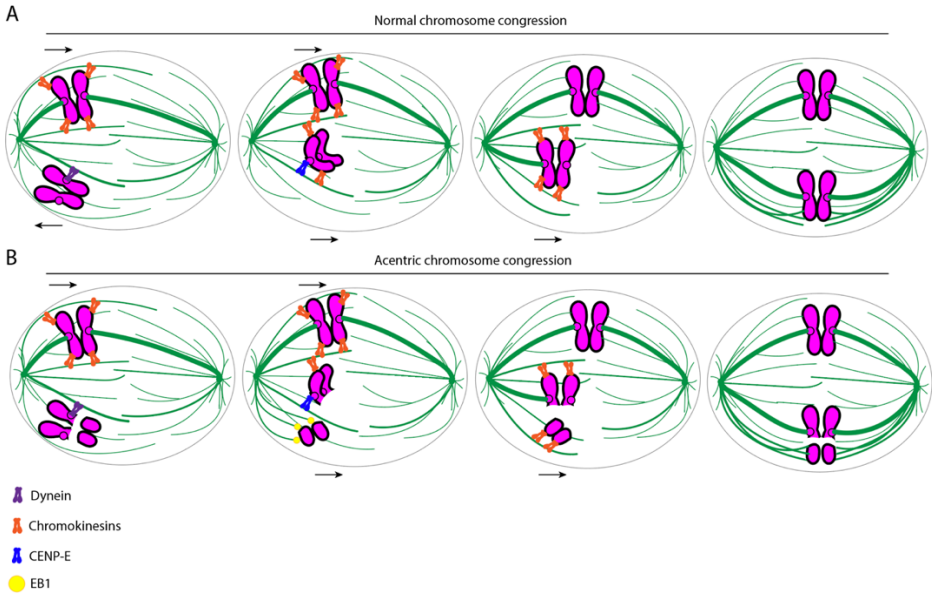
Figure 3.7: Schematic showing proposed mechanism of acentric chromosome congression. Chromosomes in magenta, microtubules in green, dynein in purple, chromokinesins in orange, CENP-E in blue, and EB1 in yellow. (A) Normal chromosomes congress to the metaphase plate by using end-on kinetochore-microtubule attachments and chromokinesins localized at chromosome arms (direct congression) or by being carried to the spindle pole by dynein, carried to the microtubule plus ends by CENP-E and chromokinesins, and then forming end-on attachments to microtubules at the kinetochore (peripheral congression). (B) Acentric chromosome fragments may congress by using EB1-driven microtubule plus-end pushing forces and lateral attachments with microtubules (potentially via chromokinesins).

Supplemental Figures
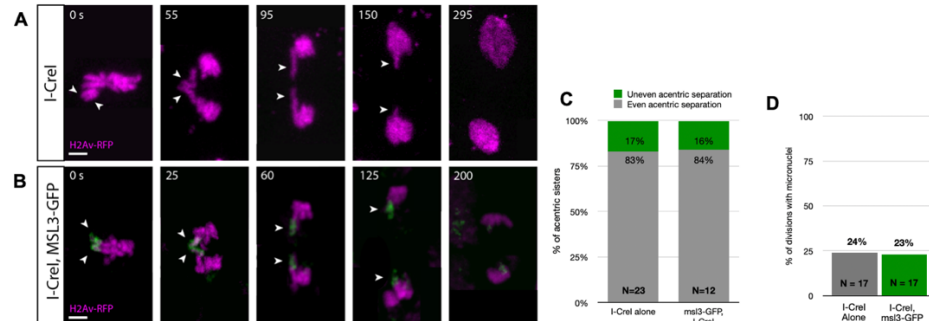
Figure S3.1: Neuroblasts expressing msl3-GFP and I-CreI behave similarly to neuroblasts only expressing I-CreI. (A) Still frames of a time-lapse movie of a mitotic neuroblast with I-CreI induced acentrics. Paired sister acentrics (white arrowheads) congress to the metaphase plate, lag behind at the spindle equator in anaphase, and eventually separate, segregate, and incorporate into daughter nuclei. (B) Still frames of a time-lapse movie of a mitotic neuroblast with I-CreI induced acentrics and expressing msl3-GFP. Bars, 2 µm. Time in seconds. (C) Percentages of acentric sisters that fail to completely separate from one another. (D) Percentages of neuroblast divisions in which acentrics failed to incorporate into daughter nuclei and formed one or more micronuclei.
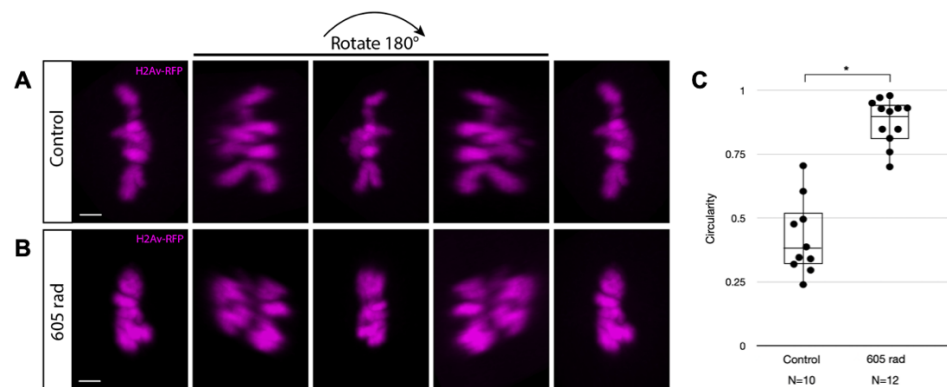
Figure S3.2: The presence of DNA damage drives the reorganization of congressed chromosomes. (A) Still images of a 3D rendering of a mitotic neuroblast expressing H2Av-RFP (magenta) with intact chromosomes. (B) Still images of a 3D rendering of a mitotic neuroblast with X-ray induced chromosome fragments. All chromosomes are arranged in a circular formation immediately prior to anaphase onset. Bars, 2 µm. Images are rotated 180°. (C) Box plot showing the circularity of the chromosome mass at metaphase immediately prior to anaphase onset. Perfect circles have a circularity of 1. Asterisks indicate statistical significance (*P=0.005) as determined by a two-sided Mann-Whitney test.
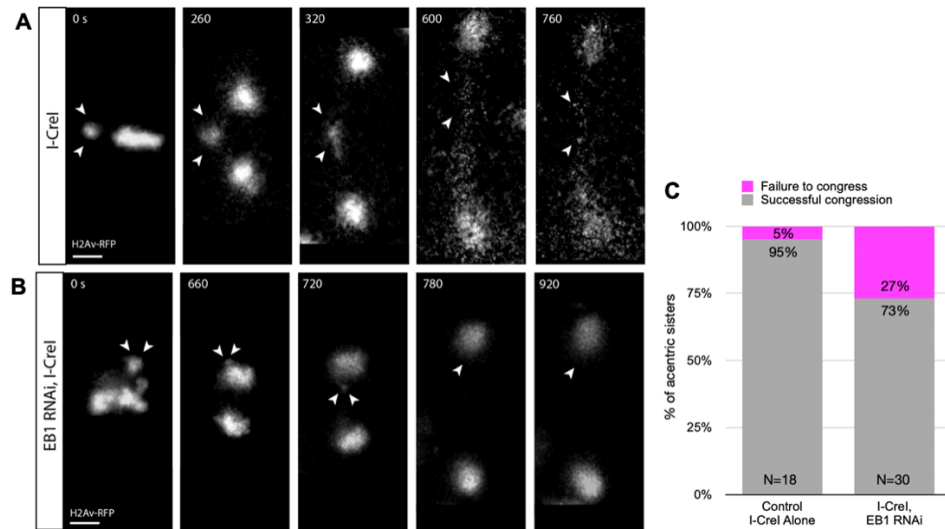
Figure S3.3: Acentrics can congress to the metaphase plate. (A) Still frames of a time-lapse movie of a mitotic neuroblast labeled with H2Av-RFP (gray) with I-CreI induced acentrics. (B) Still frames of a time-lapse movie of a mitotic neuroblast expressing I-CreI and EB1 RNAi. Sister acentrics fail to align with the chromosome mass at metaphase and segregate to the same cell pole. Bars, 2 μm. Time in seconds. (C) Bar graph showing the rate of chromosome congression to the metaphase plate. Successful chromosome congression is in gray. Failure of chromosomes to congress is in magenta.
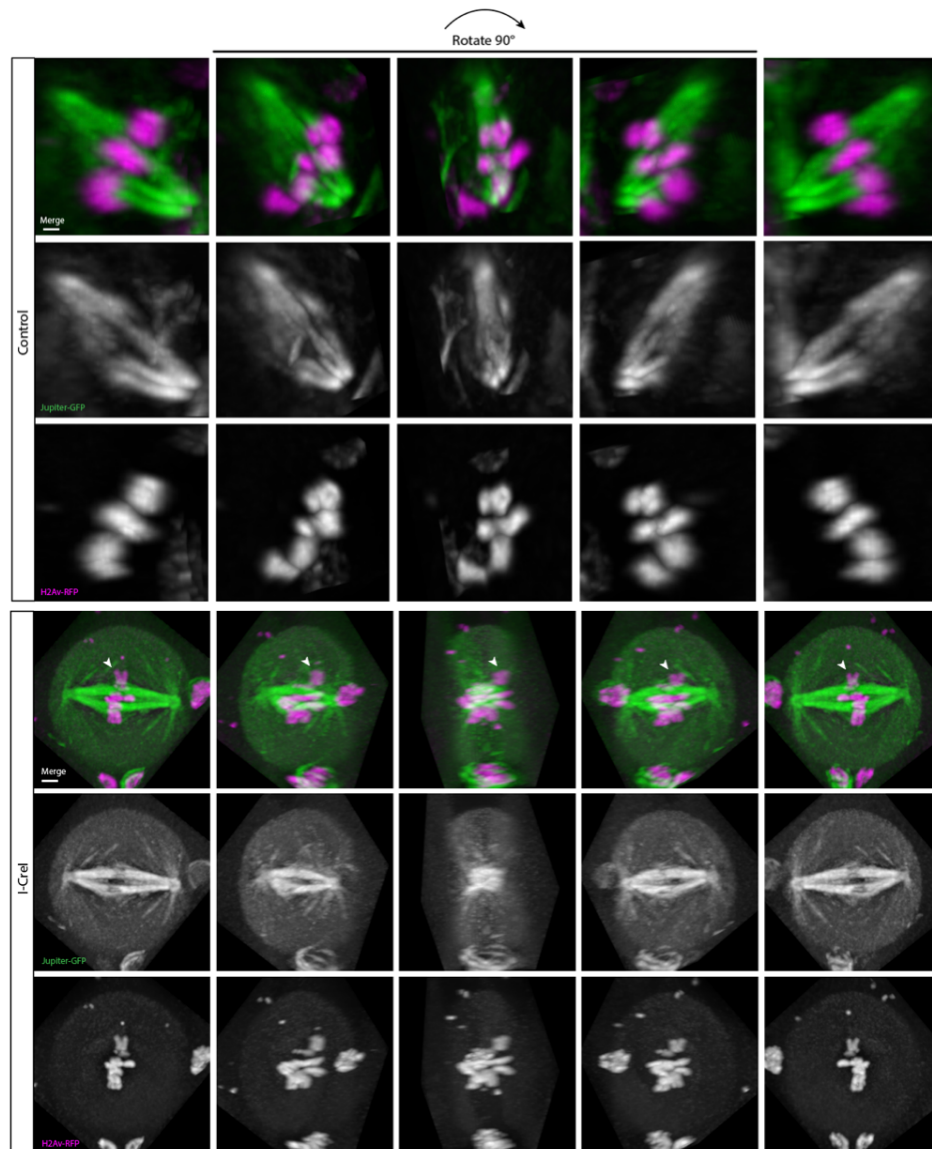
Figure S3.4: Microtubules are arranged with congressed chromosomes. A) Still images of a 3D rendering of a neuroblast at metaphase labeled with H2Av-RFP (magenta) and Jupiter-GFP (green) not expressing I-CreI. (B) Still frames of a 3D rendering of a neuroblast at metaphase with I-CreI induced acentrics. Bars, 2 μm. Images are rotated 90°.

Materials and Methods

Fly stocks

All stocks were raised on standard *Drosophila* media at room temperature (20–22˚C) as previously described [85]. For generating acentrics, a transgenic fly line bearing the I-CreI endonuclease under heat-shock 70 promoter were kindly provided by Kent Golic at The University of Utah.

Live analysis of acentric behavior in *Drosophila* third instar neuroblasts

As previously described, acentric chromosome fragments were induced by I-CreI expression (under heat shock 70 promoter) in 3rd instar larvae by a 1-hour 37˚C heat shock followed by a 1-hour recovery period at room temperature [85]. The larval brains from third instar larvae were then dissected in PBS and transferred to a slide with 20 µl of PBS. A coverslip was placed on the brain and PBS and the excess PBS was wicked out from the edges of the coverslip to induce squashing of brain between the slide and coverslip. Then, the edge of coverslip was sealed with halocarbon and was imaged for live analysis as described below. Neuroblast divisions in images for Figures 3.1, 3.2, 3.3, 3.4, 3.5, 3.6, S3.1, S3.2, S3.4, and Table 3.1 were from male 3rd instar larvae. Neuroblast divisions in images for Figure S3.3 were from female 3rd instar larvae.

Microscopy and image acquisition

Wide-field microscopy. Time-lapse imaging for Figure S3.3 was performed using a Leica DM16000B wide-field inverted microscope equipped with a Hamamatsu electron-multiplying charge coupled device camera (ORCA 9100–02) with a binning of 1 and a 100x Plan-Apochromat objective with NA 1.4. Successive time points were filmed at 20 second intervals. RFP (585 nm) and

GFP (508 nm) fluorophores were imaged. Samples were imaged in PBS and at room temperature (20–22˚C). Widefield images were acquired with Leica Application Suite Advanced Fluorescence Software and 3D deconvolved using AutoQuant X2.2.0 software.

Spinning-disk microscopy. Images in Figures 3.1, 3.2, 3.3, 3.4, 3.5, 3.6, S3.1, S3.2, and S3.4 were acquired with an inverted Nikon Eclipse TE2000-E spinning disk (CSLI-X1) confocal microscope equipped with a Hamamatsu electron-multiplying charge coupled device camera (ImageEM X2) with a 100X 1.4 NA oil-immersion objective. Samples were imaged in PBS and at room temperature (20–22˚C). Images were acquired with MicroManager 1.4 software. Time-lapse fluorescent images of neuroblasts divisions were done with 120 and 100 ms exposures for GFP and RFP respectively with 0.5 μm Z-steps. Time-lapse videos with both GFP and RFP were done every 5 seconds and time-lapse movies with RFP alone were done every 5 seconds. Figures were assembled in Adobe Illustrator. Selected stills (both experimental and control) were processed with ImageJ (http://rsb.info.nih.gov/ij/)).

X-ray Irradiation

To induce nonspecific chromosomal breaks for Figure S3.2, 3rd instar *Drosophila* larvae were subjected to 605 rad of X-ray radiation using a Precision MultiRad160 irradiator followed by a 1-hour recovery period. The larval brains were then dissected and imaged as described above.

Measurements

In Figures 3.3 and S3.2, circularity measurements of chromosomes (H2Av-RFP) were done using the circularity function in ImageJ of the region outlined around acentrics and the main mass of chromosomes. For statistical analyses, two-sided

71

Mann-Whitney-Wilcoxon tests were used. Two-sided Mann-Whitney-Wilcoxon

tests were performed in R (R Core Team) and Prism Version 8 (GraphPad

Software). 3D renderings in Figures 3.2, 3.3, S3.2, and S3.4 were created using

Imaris software.

References

1.   Afshar K, Barton NR, Hawley RS, Goldstein LSB. DNA binding and meiotic chromosomal localization of the Drosophila nod kinesin-like protein. Cell. 1995; 81:129–138. https://doi.org/10.1016/0092-8674(95)90377-1 PMID: 7720068.

2.   Archambault V, D'Avino PP, Deery MJ, Lilley KS, Glover DM. Sequestration of Polo kinase to microtubules by phosphopriming-independent binding to Map205 is relieved by phosphorylation at a CDK site in mitosis. Genes Dev. 2008; 22(19):2707–20. https://doi.org/10.1101/gad.486808 PMID: 18832073; PubMed Central PMCID: PMC2559908.

3.   Asbury CL. Anaphase A: Disassembling Microtubules Move Chromosomes toward Spindle Poles. Biology. 2017; 6(1):15. https://doi.org/10.3390/biology6010015 PMID: 28218660; PubMed Central PMCID: PMC5372008.

4.   Bajer A. Cine-micrographic studies on chromosome movements in β-irradiated cell. Chromosoma.1958; 9:319–331. PMID: 13608834.

5.   Bajer A, Vantard M. Microtubule dynamics determine chromosome lagging and transport of acentric fragments. Mutat Res. 1988; 201:271–281. https://doi.org/10.1016/0027-5107(88)90016-4

6.   Bakhoum SF, Kabeche L, Compton DA, Powell SN, Bastians H. Mitotic DNA Damage Response: At the Crossroads of Structural and Numerical Cancer Chromosome Instabilities. Trends Cancer. 2017 Mar;3(3):225-234. doi: 10.1016/j.trecan.2017.02.001. Epub 2017 Feb 28. PMID: 28718433; PMCID: PMC5518619.

7.   Baxter J, Sen N, Martinez VL, De Carandini MEM, Schvartzman JB, Diffley JFX, et al. Positive Supercoiling of Mitotic DNA Drives Decatenation by Topoisomerase II in Eukaryotes. Science. 2011; 331 (6022):1328–32. https://doi.org/10.1126/science.1201538 PMID: 21393545.

8.   Bonassi S, El-Zein R, Bolognesi C, Fenech M. Micronuclei frequency in peripheral blood lymphocytes and cancer risk: evidence from human studies. Mutagenesis. 2011 Jan;26(1):93-100. doi: 10.1093/mutage/geq075. PMID: 21164188.

9.   Bretscher HS, Fox DT. Proliferation of Double Strand Break Resistant Polyploid Cells Requires Drosophila FANCD2. Dev Cell. 2016; 37(5):444–57. https://doi.org/10.1016/j.devcel.2016.05.004 PMID: 27270041; PubMed Central PMCID: PMC4901310.

10.   Brodsky MH, Weinert BT, Tsang G, Rong YS, McGinnis NM, Golic KG, Rio DC, Rubin GM. Drosophila melanogaster MNK/Chk2 and p53 regulate multiple DNA repair and apoptotic pathways following DNA damage. 2004. https://doi.org/10.1128/mcb.24.3.1219-1231.2004

11.   Carlson JG Mitotic behavior of induced chromosomal fragments lacking spindle attachments in the neuroblasts of the grasshopper. Proc Natl Acad Sci USA. 1938a; 24:500–507. https://doi.org/10.1073/pnas.24.11.500

12.   Cenci G, Siriaco G, Raffa GD, Kellum R, Gatti M. The Drosophila HOAP protein is required for telomere capping. Nat Cell Biol. 2003; 5(1):82–4. https://doi.org/10.1038/ncb902 PMID: 12510197.

13.   Cohen-Fix O. The making and breaking of sister chromatid cohesion. Cell. 2001 Jul 27;106(2):137-40. doi: 10.1016/s0092-8674(01)00439-1. PMID: 11511341.

14.   Corona DFV, Eberharter A, Budde A, Deuring R, Ferrari S, Varga-Weisz P, et al. Two histone fold proteins, CHRAC-14 and CHRAC-16, are developmentally regulated subunits of chromatin accessibility complex (CHRAC). EMBO J. 2000; 19(12):3049–59. https://doi.org/10.1093/emboj/19.12.3049 PMID: 10856248; PubMed Central PMCID: PMC203371.

15.   Coutelier H, Xu Z. Adaptation in replicative senescence: a risky business. Curr Genet. 2019; 65(3):711–6. https://doi.org/10.1007/s00294-019-00933-7 PMID: 30637477.

16.   Ding ZM, Zhang SX, Jiao XF, Hua LP, Ahmad MJ, Wu D, Chen F, Wang YS, Zhang XY, Meng F, Duan ZQ, Miao YL, Huo LJ. Doxorubicin Exposure Affects Oocyte Meiotic Maturation through DNA Damage-Induced Meiotic Arrest. Toxicol   Sci. 2019 Oct 1;171(2):359-368. doi: 10.1093/toxsci/kfz161. PMID: 31368505.

17.   Drpic D, Almeida AC, Aguiar P, Renda F, Damas J, Lewin HA, Larkin DM, Khodjakov A, Maiato H. Chromosome Segregation Is Biased by Kinetochore Size. Curr Biol. 2018 May 7;28(9):1344-1356.e5. doi: 10.1016/j.cub.2018.03.023. Epub 2018 Apr 26. PMID: 29706521; PMCID: PMC5954971.

18.   Eissenberg JC, Elgin SCR. HP1a: A Structural Chromosomal Protein Regulating Transcription. Trends Genet. 2014; 30(3):103–10. https://doi.org/10.1016/j.tig.2014.01.002 PMID: 24555990; PubMed Central PMCID: PMC3991861.

19.   Ermolaeva MA, Schumacher B. Systemic DNA damage responses: Organismal adaptations to genome instability. Trends Genet. 2014; 30(3):95–102. https://doi.org/10.1016/j.tig.2013.12.001 PMID:24439457; PubMed Central PMCID: PMC4248340.

20.   Falck GC, Catalán J, Norppa H. Nature of anaphase laggards and micronuclei in female cytokinesis-blocked lymphocytes. Mutagenesis. 2002; 17:111–117. https://doi.org/10.1093/mutage/17.2.111

21.   Farcas A-M, Uluocak P, Helmhart W, Nasmyth K. Cohesin's Concatenation of Sister DNAs Maintains Their Intertwining. Mol Cell.

2011; 44(1–3):97–107. https://doi.org/10.1016/j.molcel.2011.07.034
PMID: 21981921; PubMed Central PMCID: PMC3240746.

22.   Feller C, Forne´ I, Imhof A, Becker PB. Global and Specific Responses
        of the Histone Acetylome to Systematic Perturbation. Molecular Cell.
        2015; 57(3):559–71. https://doi.org/10.1016/j.molcel.2014.12.008 PMID:
        25578876.

23.   Fenech M, Kirsch-Volders M, Natarajan AT, Surralles J, Crott JW, Parry
        J, et al. Molecular mechanisms of micronucleus, nucleoplasmic bridge
        and nuclear bud formation in mammalian and human cells. Mutagenesis.
        2011; 26(1):125–32. https://doi.org/10.1093/mutage/geq052 PMID:
        21164193

24.   Fogarty P, Campbell SD, Abu-Shumays R, Phalle BS, Yu KR, Uy GL,
        Goldberg ML, Sullivan W. The Drosophila grapes gene is related to
        checkpoint gene chk1/rad27 and is required for late syncytial division
        fidelity. Curr Biol. 1997 Jun 1;7(6):418-26. doi: 10.1016/s0960-
        9822(06)00189-8. PMID: 9197245.

25.   Fuge H. Anaphase transport of akinetochoric fragments in tipulid
        spermatocytes. Electron microscopic observations on fragment-spindle
        interactions. Chromosoma. 1975; 52:149–158.
        https://doi.org/10.1007/bf00326264

26.   Fuge H. Non-kinetochore transport phenomena, microtubule-
        chromosome associations, and force transmission in nuclear division.
        Protoplasma. 1990; 158:1–9.

27.   Gimenez-Abian JF, Weingartner M, Binarova P, Clarke DJ, Anthony RG,
        Calderini O, et al., A Topoisomerase II-Dependent Checkpoint in G2-
        Phase Plant Cells Can Be Bypassed by Ectopic Expression of Mitotic
        Cyclin B2, Cell Cycle. 2002; 1:3, 186-191, DOI: 10.4161/cc.1.3.124

28.   Golic MM, Golic KG. A simple and rapid method for constructing ring-X
        chromosomes in Drosophila melanogaster. Chromosoma. 2011;
        120(2):159–64. https://doi.org/10.1007/s00412-010-0297-2
        PMID:21085980; PubMed Central PMCID: PMC4454366.

29.   Goshima G, Vale RD. The roles of microtubule-based motor proteins in
        mitosis: comprehensive RNAi analysis in the Drosophila S2 cell line. J
        Cell Biol. 2003 Sep 15;162(6):1003-16. doi: 10.1083/jcb.200303022.
        PMID: 12975346; PMCID: PMC2172859.

30.   Guacci V, Koshland D, Strunnikov A. A Direct Link between Sister
        Chromatid Cohesion and Chromosome Condensation Revealed through
        the Analysis of MCD1 in S. cerevisiae. Cell. 1997; 91(1):47–57.
        https://doi.org/10.1016/s0092-8674(01)80008-8 PMID: 9335334;
        PubMed Central PMCID: PMC2670185.

31.   Gutiérrez-Caballero C, Cebollero LR, Pendás AM. Shugoshins: from
        protectors of cohesion to versatile adaptors at the centromere. Trends

Genet. 2012 Jul;28(7):351-60. doi: 10.1016/j.tig.2012.03.003. Epub 2012 Apr 27. PMID: 22542109.

32.   Hayden JH, Bowser SS, Rieder CL. Kinetochores capture astral microtubules during chromosome attachment to the mitotic spindle: direct visualization in live newt lung cells. J Cell Biol. 1990 Sep;111(3):1039-45. doi: 10.1083/jcb.111.3.1039. PMID: 2391359; PMCID: PMC2116290.

33.   Heald R, Tournebize R, Blank T, Sandaltzopoulos R, Becker P, Hyman A, et al. Self-organization of microtubules into bipolar spindles around artificial chromosomes in Xenopus egg extracts. Nature. 1996; 382(6590):420–5. https://doi.org/10.1038/382420a0 PMID: 8684481.

34.   Hentrich C, Surrey T. Microtubule organization by the antagonistic mitotic motors kinesin-5 and kinesin-14. J Cell Biol. 2010 May 3;189(3):465-80. doi: 10.1083/jcb.200910125. PMID: 20439998; PMCID: PMC2867311.

35.   Ishii K, Ogiyama Y, Chikashige Y, Soejima S, Masuda F, Kakuma T, et al. Heterochromatin Integrity Affects Chromosome Reorganization After Centromere Dysfunction. Science. 2008; 321(5892):1088–91. https://doi.org/10.1126/science.1158699 PMID: 18719285.

36.   Kanda T, Otter M, Wahl GM. Mitotic segregation of viral and cellular acentric extrachromosomal molecules by chromosome tethering. J Cell Sci. 2001; 114:49–58. PMID: 11112689.

37.   Kanda T, Sullivan KF, Wahl GM Histone-GFP fusion protein enables sensitive analysis of chromosome dynamics in living mammalian cells. Curr Biol. 1998; 8:377–385. https://doi.org/10.1016/s0960-9882(98)70156-3

38.   Kanda T, Wahl GM. The dynamics of acentric chromosomes in cancer cells revealed by GFP- based chromosome labeling strategies. J Cell Biochem Suppl. 2000; Suppl 35:107–14. https://doi.org/10.1002/1097-4644(2000)79:35+<107::aid-jcb1133>3.0.co;2-y PMID: 11389539.

39.   Karg T. Worst Case Scenario: Exiting Metaphase With a Broken Chromosome. [Doctoral Dissertation]. University of California, Santa Cruz. 2016; ProQuest Dissertations and Theses Database.

40.   Karg T, Elting MW, Vicars H, Dumont S, Sullivan W. The chromokinesin Klp3a and microtubules facilitate acentric chromosome segregation. J Cell Biol. 2017; 216(6):1597–608. https://doi.org/10.1083/jcb.201604079 PMID: 28500183; PubMed Central PMCID: PMC5461011.

41.   Karg T, Warecki B, Sullivan W. Aurora B–mediated localized delays in nuclear envelope formation facilitate inclusion of late-segregating chromosome fragments. Mol Biol Cell. 2015; 26(12):2227–41. https://doi.org/10.1091/mbc.E15-01-0026 PMID: 25877868; PubMed Central PMCID: PMC4462941.

42.   Kaye JA, Melo JA, Cheung SK, Vaze MB, Haber JE, Toczyski DP. DNA breaks promote genomic instability by impeding proper chromosome segregation. Curr Biol. 2004; 14:2096–2106. https://doi.org/10.1016/j.cub.2004.10.051

43.   Kenney RD, Heald R. Essential roles for cohesin in kinetochore and spindle function in Xenopus egg extracts. Journal of Cell Science. 2006; 119(24):5057–66. https://doi.org/10.1242/jcs.03277 PMID: 17158911.

44.   Khodjakov A, Cole RW, Bajer AS, Rieder CL. The force for poleward chromosome motion in Haemanthus cells acts along the length of the chromosome during metaphase but only at the kinetochore during anaphase. J Cell Biol. 1996; 132(6):1093–104. https://doi.org/10.1083/jcb.132.6.1093 PMID: 8601587; PubMed Central PMCID: PMC2120764.

45.   Khodjakov A, Rieder CL. Kinetochores moving away from their associated pole do not exert a significant pushing force on the chromosome. J Cell Biol. 1996; 135:315–327. https://doi.org/10.1083/jcb.135.2.315

46.   Laband K, Le Borgne R, Edwards F, Stefanutti M, Canman JC, Verbavatz JM, et al. Chromosome segregation occurs by microtubule pushing in oocytes. Nature Comm. 2017; 8(1):1499. https://doi.org/10.1038/s41467-017-01539-8 PMID: 29133801; PubMed Central PMCID: PMC5684144.

47.   LaFountain JR Jr, Cole RW, Rieder CL. Polar ejection forces are operative in crane-fly spermatocytes, but their action is limited to the spindle periphery. Cell Motil Cytoskeleton. 2002a; 5:16–26. https://doi.org/10.1002/cm.10011

48.   LaFountain JR, Oldenbourg R, Cole RW, Rieder CL. Microtubule Flux Mediates Poleward Motion of Acentric Chromosome Fragments during Meiosis in Insect Spermatocytes. Mol Biol Cell. 2001; 12 (12):4054–65. https://doi.org/10.1091/mbc.12.12.4054 PMID: 11739800; PubMed Central PMCID: PMC60775.

49.   Lewis CW, Golsteyn RM. Cancer cells that survive checkpoint adaptation contain micronuclei that harbor damaged DNA. Cell Cycle. 2016 Nov 16;15(22):3131-3145. doi: 10.1080/15384101.2016.1231287. Epub 2016 Sep 16. PMID: 27636097; PMCID: PMC5134707.

50.   Liang H, Wright WH, Cheng S, He W, Berns MW. Micromanipulation of chromosomes in PTK2 cells using laser microsurgery (optical scalpel) in combination with laser-induced optical force (optical tweezers). Experimental cell research. 1993; 204(1):110–20. https://doi.org/10.1006/excr.1993.1015 PMID: 8416789.

51.   Lisby M, Rothstein R. Cell biology of mitotic recombination. Cold Spring Harb Perspect Biol. 2015 Mar 2;7(3):a016535. doi: 10.1101/cshperspect.a016535. PMID: 25731763; PMCID: PMC4355273.

52.   Maggert KA, Golic KG. Highly Efficient Sex Chromosome Interchanges Produced By I-CreI Expression in Drosophila. Genetics. 2005; 171(3):1103–14. https://doi.org/10.1534/genetics.104.040071 PMID:16020774; PubMed Central PMCID: PMC1456814.

53.   Maiato H, Gomes AM, Sousa F, Barisic M. Mechanisms of Chromosome Congression during Mitosis. Biology (Basel). 2017 Feb 17;6(1):13. doi: 10.3390/biology6010013. PMID: 28218637; PMCID: PMC5372006.

54.   Marangos P, Stevense M, Niaka K, Lagoudaki M, Nabti I, Jessberger R, Carroll J. DNA damage-induced metaphase I arrest is mediated by the spindle assembly checkpoint and maternal age. Nat Commun. 2015 Nov 2;6:8706. doi: 10.1038/ncomms9706. PMID: 26522734; PMCID: PMC4667640.

55.   Masrouha N, Yang L, Hijal S, Larochelle S, Suter B. The Drosophila chk2 gene loki is essential for embryonic DNA double-strand-break checkpoints induced in S phase or G2. Genetics. 2003 Mar;163(3):973-82. doi: 10.1093/genetics/163.3.973. PMID: 12663536; PMCID: PMC1462500.

56.   McVey M, Andersen SL, Broze Y, Sekelsky J. Multiple Functions of Drosophila BLM Helicase in Maintenance of Genome Stability. Genetics. 2007; 176(4):1979–92. https://doi.org/10.1534/genetics.106.070052 PMID: 17507683; PubMed Central PMCID: PMC1950607.

57.   Melnikova L, Biessmann H, Georgiev P. The Ku Protein Complex Is Involved in Length Regulation of Drosophila Telomeres. Genetics. 2005; 170(1):221–35. https://doi.org/10.1534/genetics.104.034538 PMID: 15781709; PubMed Central PMCID: PMC1449706.

58.   Michaelis C, Ciosk R, Nasmyth K. Cohesins: Chromosomal Proteins that Prevent Premature Separation of Sister Chromatids. Cell. 1997; 91(1):35–45. https://doi.org/10.1016/s0092-8674(01)80007-6 PMID: 9335333.

59.   Mikhailov A, Cole RW, Rieder CL. DNA Damage during Mitosis in Human Cells Delays the Metaphase/Anaphase Transition via the Spindle-Assembly Checkpoint. Current Biology. 2002; 12(21):1797–806. https://doi.org/10.1016/s0960-9822(02)01226-5 PMID: 12419179

60.   Moon W, Hazelrigg T. The Drosophila Microtubule-Associated Protein Mini Spindles Is Required for Cytoplasmic Microtubules in Oogenesis. Current Biology. 2004; 14(21):1957–61. https://doi.org/10.1016/j.cub.2004.10.023 PMID: 15530399.

61.   Murray AW, Szostak JW. Chromosome Segregation in Mitosis and Meiosis. Annual Review of Cell Biology. 1985; 1(1):289–315. https://doi.org/10.1146/annurev.cb.01.110185.001445 PMID: 3916318.

62.   Navarro AP, Cheeseman IM. Kinetochore assembly throughout the cell cycle. Semin Cell Dev Biol. 2021 Sep; 117:62-74. doi:

10.1016/j.semcdb.2021.03.008. Epub 2021 Mar 19. PMID: 33753005; PMCID: PMC8384650.

63.   Nehlig A, Molina A, Rodrigues-Ferreira S, Honore´ S, Nahmias C. Regulation of end-binding protein EB1 in the control of microtubule dynamics. Cell Mol Life Sci. 2017; 74(13):2381–93. https://doi.org/10.1007/s00018-017-2476-2 PMID: 28204846.

64.   Nowsheen S, Yang ES. The intersection between DNA damage response and cell death pathways. Exp Oncol. 2012; 34:243–254

65.   Ohno Y, Ogiyama Y, Kubota Y, Kubo T, Ishii K. Acentric chromosome ends are prone to fusion with functional chromosome ends through a homology-directed rearrangement. Nucleic Acids Res. 2016; 44(1):232–44. https://doi.org/10.1093/nar/gkv997 PMID: 26433224; PubMed Central PMCID: PMC4705696.

66.   Oikemus SR, McGinnis N, Queiroz-Machado J, Tukachinsky H, Takada S, Sunkel CE, et al. Drosophila atm/telomere fusion is required for telomeric localization of HP1 and telomere position effect. Genes Dev. 2004; 18(15):1850–61. https://doi.org/10.1101/gad.1202504 PMID: 15256487; PubMed Central PMCID: PMC517405.

67.   Oliveira RA, Hamilton RS, Pauli A, Davis I, Nasmyth K. Cohesin cleavage and Cdk inhibition trigger formation of daughter nuclei. Nat Cell Biol. 2010; 12(2):185–92. https://doi.org/10.1038/ncb2018 PMID: 20081838; PubMed Central PMCID: PMC3284228.

68.   Oliveira RA, Kotadia S, Tavares A, Mirkovic M, Bowlin K, Eichinger CS, et al. Centromere- Independent Accumulation of Cohesin at Ectopic Heterochromatin Sites Induces Chromosome Stretching during Anaphase. PLoS Biol. 2014; 12(10):e1001962. https://doi.org/10.1371/journal.pbio.1001962 PMID: 25290697; PubMed Central PMCID: PMC4188515.

69.   Ono M, Preece D, Duquette ML, Forer A, Berns MW Mitotic tethers connect sister chromosomes and transmit "cross-polar" force during anaphase A of mitosis in PtK2 cells. Biomed Opt Express. 2017; 8:4310–4315. https://doi.org/10.1364/BOE.8.004310

70.   O'Tousa J. Meiotic chromosome behavior influenced by mutation-altered disjunction in Drosophila melanogaster females. Genetics. 1982; 102:503–524. PMID: 6816677; PubMed Central PMCID: PMC1201954.

71.   Paredes S, Maggert KA. Ribosomal DNA contributes to global chromatin regulation. Proc Natl Acad Sci USA. 2009; 106(42):17829–34. https://doi.org/10.1073/pnas.0906811106 PMID: 19822756; PubMed Central PMCID: PMC2764911.

72.   Park I, Park KK, Park JH, Chung WY. Isoliquiritigenin induces G2 and M phase arrest by inducing DNA damage and by inhibiting the metaphase/anaphase transition. Cancer Lett. 2009 May 18;277(2):174-

81. doi: 10.1016/j.canlet.2008.12.005. Epub 2009 Jan 23. PMID: 19167809.

73.   Pauletti G, Lai E, Attardi G. Early appearance and long-term persistence of the submicroscopic extrachromosomal elements (amplisomes) containing the amplified DHFR genes in human cell lines. Proc Natl Acad Sci USA. 1990 Apr;87(8):2955-9. doi: 10.1073/pnas.87.8.2955. PMID: 2326258; PMCID: PMC53812.

74.   Paulson JR, Hudson DF, Cisneros-Soberanis F, Earnshaw WC. Mitotic chromosomes. Semin Cell Dev Biol. 2021 Sep;117:7-29. doi: 10.1016/j.semcdb.2021.03.014. Epub 2021 Apr 6. PMID: 33836947; PMCID: PMC8406421.

75.   Pesavento PA, Stewart RJ, Goldstein LS. Characterization of the KLP68D kinesin-like protein in Drosophila: possible roles in axonal transport. The Journal   of Cell Biology. 1994; 127(4):1041–8. https://doi.org/10.1083/jcb.127.4.1041 PMID: 7525600; PubMed Central PMCID: PMC2200055.

76.   Pickett-Heaps JD, McDonald KL, Tippit DH. Cell division in the pennate diatom Diatom vulgare. Protoplasma. 1975; 86, 205-242.

77.   Piskadlo E, Oliveira RA. A Topology-Centric View on Mitotic Chromosome Architecture. Int J Mol Sci. 2017; 18(12):2751. https://doi.org/10.3390/ijms18122751 PMID: 29258269; PubMed Central PMCID: PMC5751350.

78.   Platero JS, Ahmad K, Henikoff S. A Distal Heterochromatic Block Displays Centromeric Activity When Detached from a Natural Centromere. Molecular Cell. 1999; 4(6):995–1004. https://doi.org/10.1016/s1097-2765(00)80228-2 PMID: 10635324.

79.   Porter ACG, Farr CJ. Topoisomerase II: untangling its contribution at the centromere. Chromosome Res. 2004; 12(6):569–83. https://doi.org/10.1023/B:CHRO.0000036608.91085.d1 PMID: 15289664.

80.   Rahal R, Amon A. Mitotic CDKs control the metaphase-anaphase transition and trigger spindle elongation. Genes Dev. 2008 Jun 1;22(11):1534-48. doi: 10.1101/gad.1638308. PMID: 18519644; PMCID: PMC2418589.

81.   Rogers SL, Rogers GC, Sharp DJ, Vale RD. Drosophila EB1 is important for proper assembly, dynamics, and positioning of the mitotic spindle. J Cell Biol. 2002; 158(5):873–84. https://doi.org/10.1083/jcb.200202032 PMID: 12213835; PubMed Central PMCID: PMC2173155.

82.   Rhind N, Russell P. Chk1 and Cds1: linchpins of the DNA damage and replication checkpoint pathways. J Cell Sci. 2000 Nov;113 (Pt 22)(Pt 22):3889-96. doi: 10.1242/jcs.113.22.3889. PMID: 11058076; PMCID: PMC2863124.

83.   Rieder CL, Davison EA, Jensen LC, Cassimeris L, Salmon ED. Oscillatory movements of monooriented chromosomes and their position relative to the spindle pole result from the ejection properties of the aster and half-spindle. J Cell Biol. 1986 Aug;103(2):581-91. doi: 10.1083/jcb.103.2.581. PMID: 3733881; PMCID: PMC2113830.

84.   Rong YS, Titen SW, Xie HB, Golic MM, Bastiani M, Bandyopadhyay P, et al. Targeted mutagenesis by homologous recombination in D. melanogaster. Genes Dev. 2002; 16(12):1568–81. https://doi.org/10.1101/gad.986602 PMID: 12080094; PubMed Central PMCID: PMC186348.

85.   Royou A, Gagou ME, Karess R, Sullivan W. BubR1- and Polo-Coated DNA Tethers Facilitate Poleward Segregation of Acentric Chromatids. Cell. 2010; 140(2):235–45. https://doi.org/10.1016/j.cell.2009.12.043 PMID: 20141837; PubMed Central PMCID: PMC2969851.

86.   Royou A, Macias H, Sullivan W. The Drosophila Grp/Chk1 DNA Damage Checkpoint Controls Entry into Anaphase. Current Biology. 2005; 15(4):334–9. https://doi.org/10.1016/j.cub.2005.02.026 PMID:15723794.

87.   Royou A, McCusker D, Kellogg DR, Sullivan W. Grapes (Chk1) prevents nuclear CDK1 activation by delaying cyclin B nuclear accumulation. J Cell Biol. 2008; 183(1):63–75. https://doi.org/10.1083/jcb.200801153 PMID: 18824564; PubMed Central PMCID: PMC2557043.

88.   Santos RA, Teixeira AC, Mayorano MB, Carrara HH, Andrade JM, Takahashi CS. Basal levels of DNA damage detected by micronuclei and comet assays in untreated breast cancer patients and healthy women. Clin Exp Med. 2010 Jun;10(2):87-92. doi: 10.1007/s10238-009-0079-4. Epub 2009 Nov 10. PMID: 19902326.

89.   Saunders RDC, AvidesM do C, Howard T, Gonzalez C, Glover DM. The Drosophila Gene abnormal spindle Encodes a Novel Microtubule-associated Protein That Associates with the Polar Regions of the Mitotic Spindle. J Cell Biol. 1997; 137(4):881–90. https://doi.org/10.1083/jcb.137.4.881 PMID: 9151690; PubMed Central PMCID: PMC2139842.

90.   Savvidou E, Cobbe N, Steffensen S, Cotterill S, Heck MMS. Drosophila CAP-D2 is required for condensin complex stability and resolution of sister chromatids. Journal of Cell Science. 2005; 118(11):2529–43. https://doi.org/10.1242/jcs.02392 PMID: 15923665.

91.   Schuh M, Lehner CF, Heidmann S. Incorporation of Drosophila CID/CENP-A and CENP-C into centromeres during early embryonic anaphase. Curr Biol. 2007; 17(3):237–243. https://doi.org/10.1016/j.cub.2006.11.051 PMID: 17222555.

92.   Siddiqui SS. Metazoan motor models: kinesin superfamily in C. elegans. Traffic. 2002 Jan;3(1):20-8. doi: 10.1034/j.1600-0854.2002.30104.x. PMID: 11872139.

93. Skibbens RV. Mechanisms of sister chromatid pairing. Int Rev Cell Mol Biol. 2008;269:283-339. doi: 10.1016/S1937-6448(08)01005-8. PMID: 18779060.

94. Staeva-Vieira E, Yoo S, Lehmann R. An essential role of DmRad51/SpnA in DNA repair and meiotic checkpoint control. EMBO J. 2003; 22(21):5863–74. https://doi.org/10.1093/emboj/cdg564 PMID: 14592983; PubMed Central PMCID: PMC275421.

95. Stokes DG, Tartof KD, Perry RP. CHD1 is concentrated in interbands and puffed regions of Drosophila polytene chromosomes. Proc Natl Acad Sci USA. 1996; 93(14):7137–42. https://doi.org/10.1073/pnas.93.14.7137 PMID: 8692958; PubMed Central PMCID: PMC38949.

96. Sural TH, Peng S, Li B, Workman JL, Park PJ, Kuroda MI. The MSL3 chromodomain directs a key targeting step for dosage compensation of the Drosophila melanogaster X chromosome. Nat Struct Mol Biol. 2008 Dec;15(12):1318-25. doi: 10.1038/nsmb.1520. Epub 2008 Nov 23. PMID: 19029895; PMCID: PMC2636508.

97. Tanaka TU, Stark MJ, Tanaka K. Kinetochore capture and bi-orientation on the mitotic spindle. Nat Rev Mol Cell Biol. 2005 Dec;6(12):929-42. doi: 10.1038/nrm1764. PMID: 16341079.

98. Tanaka TU. Bi-orienting chromosomes: acrobatics on the mitotic spindle. Chromosoma. 2008 Dec;117(6):521-33. doi: 10.1007/s00412-008-0173-5. Epub 2008 Aug 2. PMID: 18677502.

99. Tao L, Mogilner A, Civelekoglu-Scholey G, Wollman R, Evans J, Stahlberg H, Scholey JM. A homotetrameric kinesin-5, KLP61F, bundles microtubules and antagonizes Ncd in motility assays. Curr Biol. 2006 Dec 5;16(23):2293-302. doi: 10.1016/j.cub.2006.09.064. PMID: 17141610.

100. Theurkauf WE, Hawley RS. Meiotic spindle assembly in Drosophila females: Behavior of nonexchange chromosomes and the effects of mutations in the nod kinesin-like protein. J Cell Biol. 1992; 116:1167–1180. https://doi.org/10.1083/jcb.116.5.1167 PMID: 1740471; PubMed Central PMCID:PMC2289365.

101. Tirnauer JS, Bierer BE. EB1 proteins regulate microtubule dynamics, cell polarity, and chromosome stability. J Cell Biol. 2000; 149(4):761–6. https://doi.org/10.1083/jcb.149.4.761 PMID: 10811817; PubMed Central PMCID: PMC2174556.

102. Titen SW, Golic KG. Telomere loss provokes multiple pathways to apoptosis and produces genomic instability in Drosophila melanogaster. Genetics. 2008 Dec;180(4):1821-32. doi: 10.1534/genetics.108.093625. Epub 2008 Oct 9. PMID: 18845846; PMCID: PMC2600924.

103. Toyoda Y, Yanagida M. Coordinated Requirements of Human Topo II and Cohesin for Metaphase Centromere Alignment under Mad2-dependent Spindle Checkpoint Surveillance. Mol Biol Cell. 2006; 17

(5):2287–302. https://doi.org/10.1091/mbc.e05-11-1089 PMID: 16510521; PubMed Central PMCID: PMC1446084.

104.   Uhlmann F, Lottspeich F, Nasmyth K. Sister-chromatid separation at anaphase onset is promoted by cleavage of the cohesin subunit Scc1. Nature. 1999; 400(6739):37–42. https://doi.org/10.1038/21831 PMID: 10403247.

105.   Uhlmann F, Wernic D, Poupart M-A, Koonin EV, Nasmyth K. Cleavage of Cohesin by the CD Clan Protease Separin Triggers Anaphase in Yeast. Cell. 2000; 103(3):375–86. https://doi.org/10.1016/s0092-8674(00)00130-6 PMID: 11081625

106.   Urban E, Nagarkar-Jaiswal S, Lehner CF, Heidmann SK. The Cohesin Subunit Rad21 Is Required for Synaptonemal Complex Maintenance, but Not Sister Chromatid Cohesion, during Drosophila Female Meiosis. PLoS Genet. 2014; 10(8):e1004540. https://doi.org/10.1371/journal.pgen.1004540 PMID: 25101996; PubMed Central PMCID: PMC4125089.

107.   Valencia-González HA, Ruíz G, Ortiz-Sánchez E, García-Carrancá A. Cancer Stem Cells from Tumor Cell Lines Activate the DNA Damage Response Pathway after Ionizing Radiation More Efficiently Than Noncancer Stem Cells. Stem Cells Int. 2019 Apr 3;2019:7038953. doi: 10.1155/2019/7038953. PMID: 31073313; PMCID: PMC6470433.

108.   Vázquez-Diez C, Yamagata K, Trivedi S, Haverfield J, FitzHarris G. Micronucleus formation causes perpetual unilateral chromosome inheritance in mouse embryos.Proc Natl Acad Sci U S A. 2016 Jan 19;113(3):626-31. doi: 10.1073/pnas.1517628112. Epub 2016 Jan 4. PMID: 26729872; PMCID: PMC4725495.

109.   Vicars H, Karg T, Warecki B, Bast I, Sullivan W. Kinetochore-independent mechanisms of sister chromosome separation. PLOS Genetics. 2021; 17(1): e1009304. doi:10.1371/journal.pgen.1009304 PMID: 33513180

110.   Vitre B, Coquelle FM, Heichette C, Garnier C, Chre´tien D, Arnal I. EB1 regulates microtubule dynamics and tubulin sheet closure in vitro. Nat Cell Biol. 2008; 10(4):415–21. https://doi.org/10.1038/ncb1703 PMID: 18364701.

111.   Voets E, Wolthuis RMF. MASTL is the human orthologue of Greatwall kinase that facilitates mitotic entry, anaphase and cytokinesis. Cell Cycle. 2010; 9(17):3591–601. https://doi.org/10.4161/cc.9.17.12832 PMID: 20818157.

112.   Wang LH-C, Mayer B, Stemmann O, Nigg EA. Centromere DNA decatenation depends on cohesin removal and is required for mammalian cell division. Journal of Cell Science. 2010; 123(5):806–13. https://doi.org/10.1242/jcs.058255 PMID: 20144989.

113. Warecki B, Ling X, Bast I, Sullivan W. ESCRT-III–mediated membrane fusion drives chromosome fragments through nuclear envelope channels. Journal of Cell Biology. 2020; 219(3):e201905091. https://doi.org/10.1083/jcb.201905091 PMID: 32032426; PubMed Central PMCID: PMC7054997.

114. Warecki B, Sullivan W. Micronuclei formation is prevented by Aurora B-mediated exclusion of HP1a from late-segregating chromatin in Drosophila. Genetics. 2018; 210(1):171–187. https://doi.org/10.1534/genetics.118.301031 PMID: 29986897; PubMed Central PMCID: PMC6116970.

115. Warecki B, Sullivan W. Mechanisms driving acentric chromosome transmission. Chromosome Res. 2020; 28(3-4):229-246. https://doi.org/10.1007/s10577-020-09636-z PMID: 32712740.

116. Ye AA, Verma V, Maresca TJ. NOD is a plus end–directed motor that binds EB1 via a new microtubule tip localization sequence. J Cell Biol. 2018; 217(9):3007–17. https://doi.org/10.1083/jcb.201708109 PMID: 29899040; PubMed Central PMCID: PMC6122986.

117. Yu J, Fleming SL, Williams B, Williams EV, Li Z, Somma P, et al. Greatwall kinase: a nuclear protein required for proper chromosome condensation and mitotic progression in Drosophila. J Cell Biol. 2004; 164:487–492. https://doi.org/10.1083/jcb.200310059 PMID: 14970188; PubMed Central PMCID: PMC2171981.

118. Zhang CZ, Spektor A, Cornils H, Francis JM, Jackson EK, Liu S, Meyerson M, Pellman D. Chromothripsis from DNA damage in micronuclei. Nature. 2015 Jun 11;522(7555):179-84. doi: 10.1038/nature14493. Epub 2015 May 27. PMID: 26017310; PMCID: PMC4742237.